Role of metal *d* states in II-VI semiconductors

S.-H. Wei and Alex Zunger
Solar Energy Research Institute, Golden, Colorado 80401
(Received 30 October 1987)

All-electron band-structure calculations and photoemission experiments on II-VI semiconductors both exhibit a metal *d* subband inside the main valence band. It has nevertheless been customary in pseudopotential and tight-binding approaches to neglect the metal *d* band by choosing Hamiltonian parameters which place this band inside the chemically inert atomic cores. Using all-electron self-consistent electronic-structure techniques (which treat the outermost *d* electrons on the same footing as other valence electrons) and comparing the results to those obtained by methods which remove the *d* band from the valence spectrum, we study their effects on valence properties. For II-VI semiconductors we find that *p-d* repulsion and hybridization (i) lower the band gaps, (ii) reduce the cohesive energy, (iii) increase the equilibrium lattice parameters, (iv) reduce the spin-orbit splitting, (v) alter the sign of the crystal-field splitting, (vi) increase the valence-band offset between common-anion II-VI semiconductors, and (vii) modify the charge distributions of various II-VI systems and their alloys. *p-d* repulsion is also shown to be responsible for the occurrence of *deep* Cu acceptor levels in II-VI semiconductors (compared with *shallow* acceptors of Zn in III-V), for the anomalously small band gaps in chalcopyrites, and for the negative exchange splitting in ferromagnetic MnTe.

I. INTRODUCTION

The electronic structure of II-VI semiconductors ZnX^{VI}, CdX^{VI}, and HgX^{VI} is distinguished from that of both column-II*A* chalcogenides CaX^{VI}, SrX^{VI}, and BaX^{VI} and from the III-V semiconductors by having a cation *d* band inside the main valence band. These valence *d* bands are evident in photoemission spectra[1-3] (Fig. 1 and Table I) and in all-electron band-structure calculations[4-11] (Figs. 2 and 3), both exhibiting a moderately narrow ($\lesssim 1$ eV), fully occupied metal *d* band around 7–11 eV below the valence-band maximum and 6–2 eV above its minimum. Whereas elements to the left of column II*B* in the Periodic Table (transition metals) are commonly considered to manifest *d*-electron effects near the Fermi energy, and the valence properties of elements to the right of column II*B* (post-transition elements) appear to be well described without explicit reference to their deep *d* bands, column-II*B* compounds constitute a borderline case. In early electronic-structure calculations for II-VI semiconductors[4-6] the metal *d* bands were retained (see also more recent results in Refs. 7–11). However, most current calculations using empirical,[12-18] semiempirical,[19] or first-principles[20,21] pseudopotential approaches, as well as tight-binding approaches[22-24] to II-VI semiconductors, their alloys,[25-29] and their impurity states[30-32] have ignored the metal *d* bands, assuming them to be a part of the chemically inert atomic cores. The underlying assumption in these approaches seems to have been that the *d* bands in II-VI semiconductors are nonbonding, energetically removed from the outer valence orbitals and difficult to treat explicitly in either pseudopotential or tight-binding methods and hence are best explicitly discarded from the spectrum (e.g., by modifying the ionic potentials[12-21] or the Hamiltonian matrix elements[22-32]) and represented only implicitly through their indirect effects on the valence *s* and *p* electrons of the constituent atoms.

In this paper we examine the extent to which the metal *d* orbitals in II-VI semiconductors can be viewed as core-like chemically inert states. We use all-electron band-structure and total-energy techniques which treat the outer metal *d* electrons on the same footing as other valence electrons. We compare the results with those in which the *d* bands are omitted or frozen. We establish the effects of these metal *d* bands on (i) band gaps, (ii) spin-orbit splittings at the valence-band maximum, (iii) ground-state properties such as equilibrium lattice parameters, cohesive energies, and bulk moduli, and (iv) valence-band offsets between semiconductors. Significant *d*-electron effects are found for all of the above.

TABLE I. Experimentally observed cation *d*-band binding energies (in eV) with respect to the valence-band maximum. When two values are given for a compound, the first corresponds to $J=\frac{5}{2}$ and the second to $J=\frac{3}{2}$ spin-orbit components.

	Ref. 1	Ref. 2	Ref. 3
ZnO, 3*d*		8.81	8.5
ZnS, 3*d*		9.03	
ZnSe, 3*d*		9.20	8.9
ZnTe, 3*d*	9.5	9.84	9.1
	9.8		
CdS, 4*d*		9.64	10.0
CdSe, 4*d*	9.55	10.04	10.7
	10.28		
CdTe, 4*d*	10.09	10.49	10.5
	10.72		
HgSe, 5*d*	7.33		
	9.13		
HgTe, 5*d*	7.70	7.87	7.6
	9.55	9.64	9.5

II. CLASSIC PHENOMENOLOGY: EFFECTS OF A "NONBONDING" d^{10} SHELL

The *global* effect of the metal d electrons on the properties of II-VI semiconductors can be assessed by comparing their properties to those of the analogous alkaline-earth compounds (which lack valence d bands).

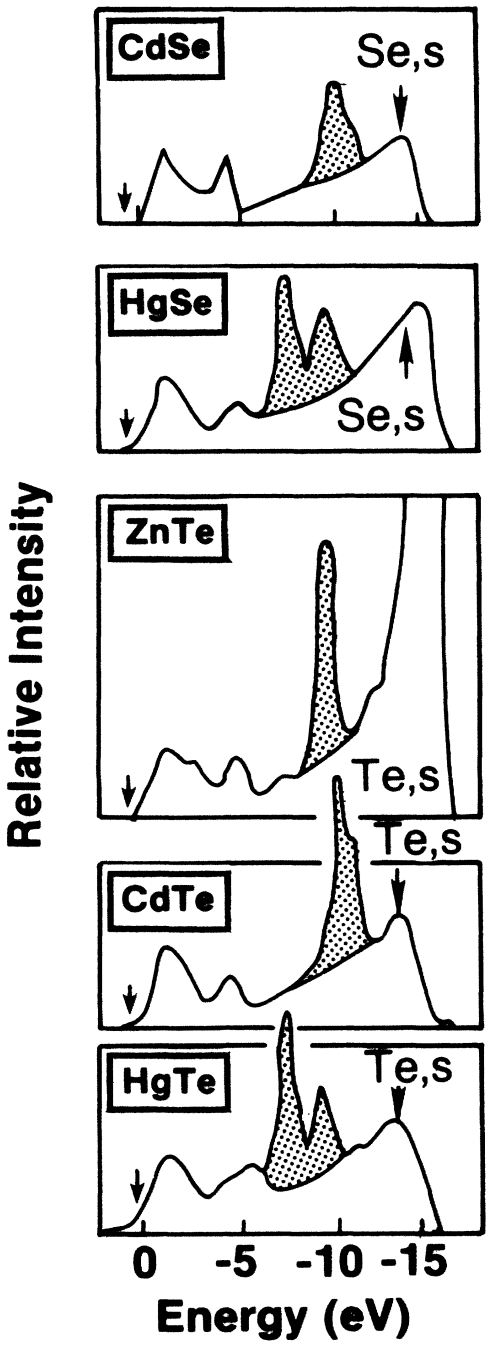

FIG. 1. Observed photoemission spectra (Refs. 1–3) of cation d states (shaded regions) in the II-VI compounds. The arrow near $E=0$ points to the valence-band maximum.

The large difference between the properties of CaX^{VI} versus ZnX^{VI}, SrX^{VI} versus CdX^{VI}, and BaX^{VI} versus HgX^{VI} (Table II),[33–39] and indeed between the chemistry of group-II A and group-II B inorganic compounds can be understood phenomenologically (e.g., see textbook discussions in Refs. 40–43): Had the d^{10}-electron shell fully compensated electrostatically for the ten added protons in going from, say ^{20}Ca to ^{30}Zn, or from ^{38}Sr to ^{48}Cd, the two members of each pair would have very similar valence properties except, perhaps, for atomic size (Zn,Cd could be *larger* than Ca,Sr, respectively, because of the added electron shell in the former case). However, since the $(n-1)d^{10}$ orbitals (with their vanishing amplitude at the nucleus) are not corelike charges (note the dispersion of their bands in Figs. 2 and 3, and the width of their photoemission bands in Fig. 1), they do not completely screen the ten added protons as far as the other valence electrons are concerned. This leaves a net attractive electron-ion potential in the II B elements in excess of that pertinent to the corresponding group-II A elements. Consequently, the valence s orbitals of the II B elements are more strongly bound to the nucleus than the corresponding s orbitals in group-II A elements (the observed[44] $s^2 \rightarrow s^1 + e$ valence ionization potentials are 6.1, 5.7, and 5.2 eV in Ca, Sr, and Ba, respectively, compared with the larger values of 9.4, 9.0, and 10.4 eV for Zn, Cd, and Hg, respectively). This imperfect d-orbital screening in group-II B compounds makes their atomic sizes and lattice parameters *smaller*[45] than those of group-II A compounds (Table II), despite the added orbital shell in the former case. The relative ease with which valence s orbitals can be removed from the atomic sites in II A elements makes them amenable to forming *ionic* II A-VI structures (all II A chalcogenides have the rocksalt structure[33]), whereas the more tightly bound valence s electrons in group-II B elements force them to form *electron-sharing* bonds which at ambient pressure stabilize the zinc-blende (or wurtzite) structure (except for HgS), and transform to the NaCl form only at higher pressures.[46] The smaller band gaps, lattice constants, and cohesive energies and the larger bulk moduli of the II B-VI semiconductors (Table II) are then direct manifestations of their reduced ionicities relative to the II A-VI compounds, a consequence of incomplete d-orbital screening effects.

The *indirect* effects of d orbitals on the properties of II B-VI semiconductors are routinely taken into account by models that explicitly neglect[12–32] the *d band* in the solid, by using sufficiently tightly bound (relative to group-II A atoms) atomic-s-orbital energies (in tight-binding models) or sufficiently attractive ionic pseudopotentials (in empirical or semiempirical pseudopotential approaches). Using adjustable parameters it is then possible to fit, for example, the calculated low-lying band gaps of such compounds to experiment. Manipulating the *atomic quantities* (atomic-orbital energies and pseudopotentials) could, however, misrepresent the direct effects of the d orbitals in the *solid-state phase,* i.e., p-d-hybridization effects which affect band baps and equilibrium structural properties. These effects are discussed next, first in a qualitative fashion (Secs. III and IV), and then quantitatively (Sec. VI).

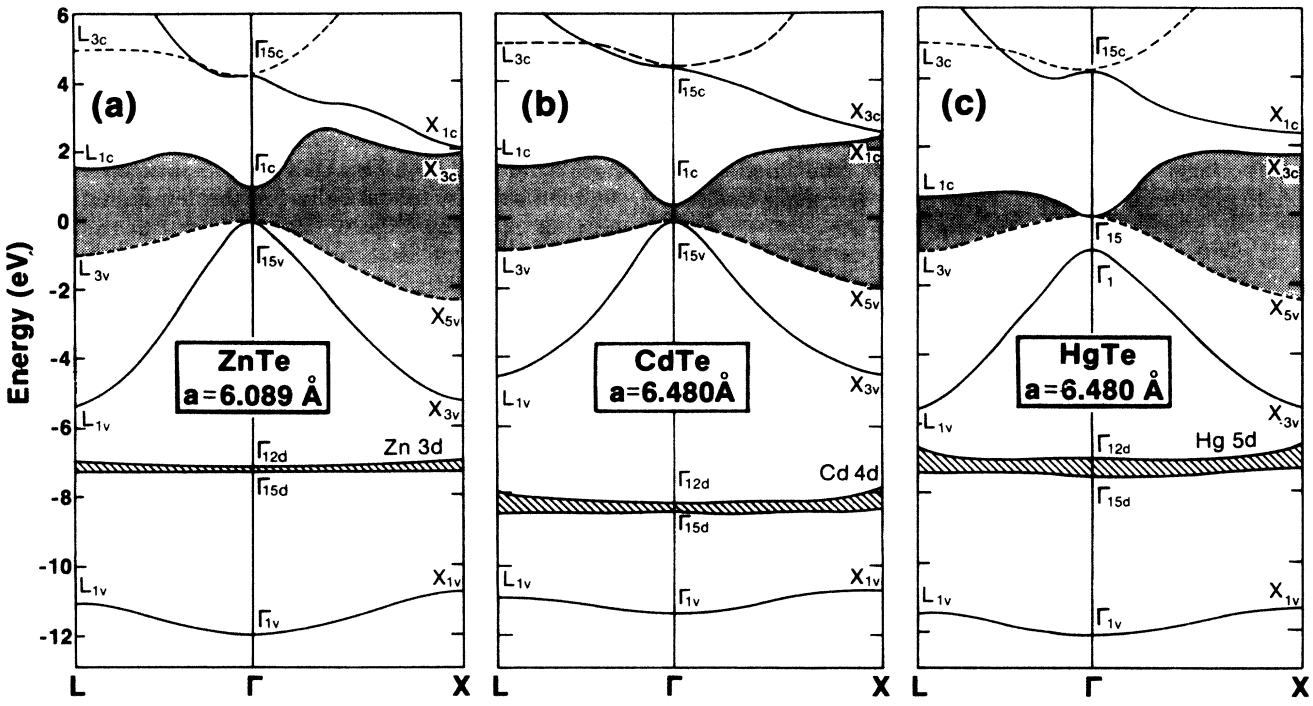

FIG. 2. Calculated (LAPW) band structure of (a) ZnTe, (b) CdTe, and (c) HgTe near their equilibrium lattice constants. The cation d bands are highlighted by the dashed lines. The band-gap regions are shaded. Dashed lines indicate doubly degenerate states.

III. *p-d* COUPLING IN TETRAHEDRAL STRUCTURE: ESSENTIAL PHYSICS

Whereas the octahedral point group (O_h) for the NaCl structure has inversion symmetry, the tetrahedral point group (T_d) pertinent to zinc-blende compounds does not. Consequently, symmetry representations of O_h do not mix even and odd angular momenta (e.g., p with d), while those of T_d do.[47] For example, whereas the band-state representations at the Brillouin-zone center in O_h symmetry show no p-d (or s-f) mixing between the central-atom d states and the ligand p states,

$$\Gamma_1[O_h]\text{: } s+g \text{ states } (l=0,4)\,, \tag{1a}$$

TABLE II. Lattice constant a (in Å), bulk modulus B (in GPa), cohesive energy E_c [in (eV)/(2 atoms)], and band gap E_g (in eV) of IIA-VI and IIB-VI compounds. The IIA-VI compounds are in the rocksalt ($B1$) structure and IIB-VI (in eV) compounds are in the zinc-blende ($B3$) structure.

IIA-VI compounds	a[a]	B[b]	E_c[c]	E_g[d]	IIB-VI compounds	a[e]	B[f]	E_c[c]	E_g[d]
CaS	5.690	43.4	9.62	5.8	ZnS	5.411	76.9	6.33	3.82
CaSe	5.91	52.1	7.90	4.9	ZnSe	5.669	62.5	5.25	2.87
CaTe	6.345	47.6	6.88	4.1	ZnTe	6.089	50.9	4.82	2.39
SrS	6.020	35.3	9.25	4.8	CdS	5.83	64.3	5.56	2.58
SrSe	6.23	45.0	8.08	4.4	CdSe	6.084	55.0	4.91	1.82
SrTe	6.47	40.5	6.64	3.7	CdTe	6.48	44.5	4.45	1.60
BaS	6.388	55.6	9.35	3.9	HgS	5.852	68.6		−0.2∼0.5
BaSe	6.600	41.5	8.22	3.6	HgSe	6.074	57.6	3.37	−0.1
BaTe	6.986	35.8	6.92	3.4	HgTe	6.460	47.6	3.22	−0.3

[a]Reference 33.
[b]Reference 34.
[c]Cohesive energies are obtained from the formation enthalpies of Ref. 35 and the elemental cohesive energies of Ref. 36.
[d]Reference 37.
[e]Reference 38.
[f]Reference 39.

$$\Gamma_{15}[O_h]\text{: } (p_x,p_y,p_z)+f \text{ states } (l=1,3)\,, \tag{1b}$$

$$\Gamma_{25'}[O_h]\text{: } (d_{xz},d_{xy},d_{yz})+g \text{ states } (l=2,4)\,, \tag{1c}$$

$$\Gamma_{12}[O_h]\text{: } (d_{3z^2-r^2},d_{x^2-y^2})+g \text{ states } (l=2,4)\,, \tag{1d}$$

in T_d symmetry such mixings are permitted, e.g.,

$$\begin{aligned}&\Gamma_1[T_d]\text{: } s+f+g \quad (l=0,3,4)\,,\\ &\Gamma_{15}[T_d]\text{: } (p_x,p_y,p_z)+(d_{xz},d_{xy},d_{yz})\\ &\qquad +f \text{ states } (l=1,2,3)\,.\end{aligned} \tag{2}$$

The fact that direct p-d mixing is symmetry forbidden in octahedral symmetry accounts for the success of the crystal-field theory for such compounds,[42,47] in which both electron interactions with the lattice and many-electron multiplet effects could be simply treated within a renormalized basis of pure, metal-atom-centered, $l=2$ [Eqs. (1c) and (1d)] Kubic harmonics (sometimes small $l=4$ corrections are added). Conversely, the fact that p-d mixing *is* symmetry allowed in tetrahedral compounds is responsible for numerous new effects.[48]

Consider, for example, a zinc-blende crystal and ignore for the moment the cation d states. The states near the band edge at Γ can be described qualitatively by a simple tight-binding model retaining the cation p orbitals (p^c with energy ε_p^c) and the anion p orbitals (p^a with energy ε_p^a). Since both have the same symmetry representation Γ_{15} (also termed t_2), they can interact [Fig. 4(a)] through a coupling matrix element V_{pp}, forming a lower-energy bonding state at the energy

$$\varepsilon(\Gamma_{15v}(p))=\frac{\varepsilon_p^c+\varepsilon_p^a}{2}-\left[\left[\frac{\varepsilon_p^a-\varepsilon_p^c}{2}\right]^2+V_{pp}^2\right]^{1/2}, \tag{3}$$

and an antibonding state at

$$\varepsilon(\Gamma_{15c}(p))=\frac{\varepsilon_p^c+\varepsilon_p^a}{2}+\left[\left[\frac{\varepsilon_p^a-\varepsilon_p^c}{2}\right]^2+V_{pp}^2\right]^{1/2}. \tag{4}$$

The bonding state has no node and its energy is lowered relative to ε_p^a [Fig. 4(a)] by this level repulsion. If, however, cation d states are included at an energy ε_d^c [Fig. 4(b)], they too have a representation of t_2 symmetry (their Γ_{12}, or e-symmetry, state cannot couple to $l=1$; hence it remains unshifted) and can couple, through a matrix element V_{pd}. This coupling can lead to (i) an inversion of the order of the d-orbital levels [$\Gamma_{15}(dp)$ below $\Gamma_{12}(d)$,

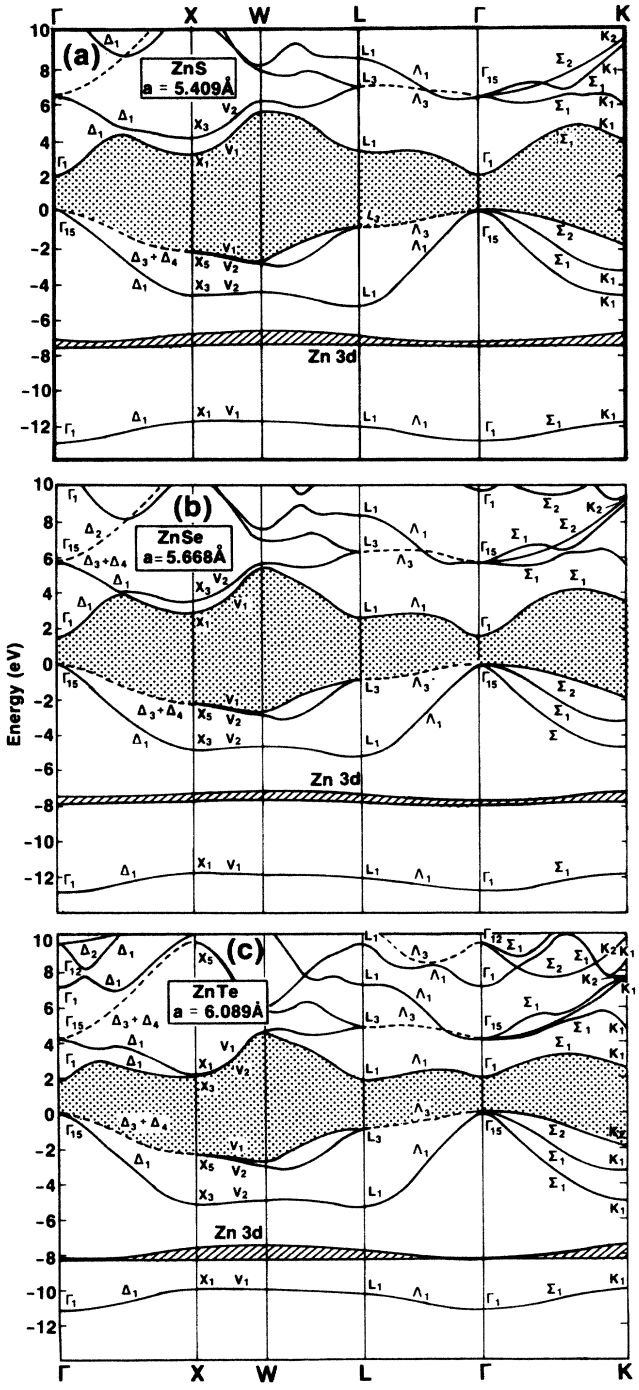

FIG. 3. Same as Fig. 2, but calculated using the nonrelativistic all-electron mixed-basis method (Ref. 10) for (a) ZnS, (b) ZnSe, and (c) ZnTe.

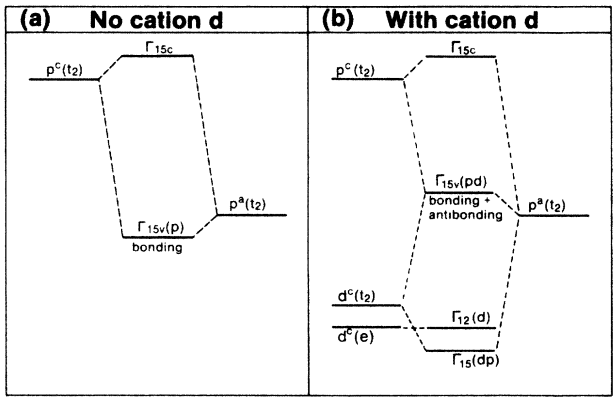

FIG. 4. Schematic plot of pp and pd coupling in zinc-blende semiconductors. (a) pp coupling only and (b) inclusion of pp and pd coupling.

TABLE III. Atomic eigenvalues (in eV) calculated by different methods. NR and SR indicate nonrelativistic and semirelativistic calculation, respectively, and HF denotes Hartree-Fock.

	HF(NR)[a]	Harrison's table[b] (NR, Herman-Skillman)	LDF[c] NR	LDF[c] SR
Zn 4*s*	−7.96	−8.40	−6.15	−6.31
4*p*	−4.02	−3.38	−1.36	−1.31
3*d*	−21.28	−17.11	−10.89	−10.48
Cd 5*s*	−7.21	−7.70	−5.65	−6.04
5*p*	−3.99	−3.38	−1.51	−1.41
5*d*	−20.76	−18.28	−12.85	−11.96
Hg 6*s*	−7.10	−7.68	−5.67	−7.21
6*p*	−3.95	−3.48	−1.56	−1.26
6*d*	−19.43	−17.27	−12.37	−10.09
S 3*s*	−24.01	−20.80	−17.24	−17.36
3*p*	−11.60	−10.27	−7.20	−7.19
Se 4*s*	−22.86	−20.32	−16.98	−17.56
4*p*	−10.68	−9.53	−6.77	−6.74
Te 5*s*	−19.12	−17.11	−14.26	−15.43
5*p*	−9.54	−8.59	−6.25	−6.19

[a]Reference 49.
[b]Ref. 22(a) and 50.
[c]Present local-density-functional (LDF) results obtained using the exchange-correlation potential of Ref. 51.

see Fig. 4(b)] relative to what is expected without *p-d* repulsion ($e=\Gamma_{12}$ below $t_2=\Gamma_{15}$, see Ref. 42), (ii) an upward shift of the $\Gamma_{15v}(pd)$ state relative to the $\Gamma_{15v}(p)$ state, and (iii) mixing of *antibonding* character into $\Gamma_{15v}(pd)$ [the valence-band maximum (VBM) in the compound].

One can estimate the magnitude of these effects semiquantitatively by considering the *p-d*-repulsion energy perturbatively, as

$$\Delta E_{pd} \sim \frac{V_{pd}^2}{\varepsilon_p^a - \varepsilon_d^c} . \tag{5}$$

The magnitude of the energy denominator can be estimated by a difference of atomic-orbital energies given in Table III.[49–51] The nonrelativistic Hartree-Fock[49(a)] or Herman-Skillman[50] orbital energies used by Harrison[22(a),49(b),49(c)] show very deep cation *d* states, producing in II-VI compounds negligible *p-d* repulsion effects (e.g., Table III, show that the HF *p-d* energy difference for ZnTe is 11.74 eV compared with 4.29 eV of the LDF results. The Zn 3*d* energy level is even lower than that of the Te 5*s* state in the HF nonrelativistic calculation). The semirelativistic local-density orbital energies of Table III, however, correctly position the *d* bands inside the main valence bands in II-VI compounds (Figs. 1–3 and Table I). Using these orbital energies one finds values of the energy denominators [Eq. (5)] shown in the first column of Table IV. For comparison, we give in the second column of this table the observed[1,2,52] metal *d* binding energies (*not eigenvalue differences*) relative to

TABLE IV. Calculated semirelativistic local-density-functional atomic-energy differences $\varepsilon_p^a - \varepsilon_d^c$ (in eV), where ε_d^c and ε_p^a are the metal-*d*-orbital and nonmetal-*p*-orbital energies, respectively. The experimental *d*-band binding energies (with respect to the VBM) are also given. We use the exchange-correlation potential of Ref. 51.

Compounds	$\varepsilon_p^a - \varepsilon_d^c$ (atoms)	Observed binding energies (solids, relative to the VBM)
GaP	13.50	18.76[a]
GaAs	13.75	18.86[a]
GaSb	14.09	18.96[a]
InP	13.07	17.41[a]
InAs	13.32	17.23[a]
InSb	13.66	17.80[a]
ZnS	3.29	9.03[b]
ZnSe	3.74	9.20[b]
ZnTe	4.29	9.84[b]
CdS	4.76	9.64[b]
CdSe	5.21	10.04[b]
CdTe	5.76	10.49[b]
HgS	2.90	
HgSe	3.35	8.05[c]
HgTe	3.90	8.58[b]

[a]Reference 52.
[b]Reference 2.
[c]Reference 1.

TABLE V. Calculated p-d-repulsion energy for ZnTe, CdTe, and HgTe using model A with three different input parameters A1, A2, and A3 (see Appendix). Results are given in eV. Here, Q_d is the fraction of d character in the metal sphere, V_{pd} is the p-d-coupling matrix element, and ΔE_{pd} [Eq. (5)] is the energy shift of the valence-band maximum due to p-d repulsion.

	ZnTe				CdTe				HgTe			
	Q_d	$\Gamma_{15v}-\Gamma_{15d}$	V_{pd}	ΔE_{pd}	Q_d	$\Gamma_{15v}-\Gamma_{15d}$	V_{pd}	ΔE_{pd}	Q_d	$\Gamma_{15v}-\Gamma_{15d}$	V_{pd}	ΔE_{pd}
Model A1	0.072	7.27	1.88	0.52	0.074	8.43	2.21	0.62	0.129	7.38	2.48	0.95
Model A2	0.049	7.27	1.56	0.35	0.049	8.43	1.82	0.41	0.092	7.38	2.14	0.68
Model A3	0.053	9.80	2.24	0.54	0.053	10.60	2.38	0.56	0.091	9.55	2.75	0.87

the valence-band maximum. These results show that the d bands in II-VI semiconductors have moved up in energy relative to the corresponding bands in III-V compounds by as much as 9–10 eV. [The relative compactness of the $(n-1)d^{10}$ orbitals makes them sample the nuclear charge far closer then the np orbitals, leading to a steep decrease in the energy of the d orbitals with atomic number, e.g., in Zn→Ga or Cd→In.] It appears that the unphysically deep d-orbital energies given by the Hartree-Fock model (Table III) was responsible for the neglect of d bands in early tight-binding models for II-VI semiconductors.[22–24]

Estimating V_{pd} from Harrison's[22(a)] formula $V_{pd}=A(r_d^{3/2}/d^{7/2})$, where r_d and d are the cation d-orbital radius[53] and the average bond length, respectively, one finds $V_{pd}\simeq 1-2$ eV. This suggests that the p-d repulsion shifts the valence-band maximum to higher energies by ΔE_{pd}, of the order of 0.1–0.3 eV for III-V compounds, but of order 1 eV for II-VI compounds. The Appendix provides other simple estimates shown in Tables V–VIII. These involve the use of two simple models to estimate the shift in the valence-band maximum due to p-d coupling: first ("model A"), using the splitting between Γ_{15v} and Γ_{15d}, and second ("model B"), using the fact that the p-d repulsion increases the overall $\Gamma_{1v}-\Gamma_{15v}$ valence-band width, as its bottom (Γ_{1v}) is unaffected by d states while its top (Γ_{15v}) is. This effect is evident from the photoemission data.[2,3(b)]

It thus appears from these simple estimates that p-d repulsion cannot be neglected in II-VI semiconductors. Quantitative calculations, using all-electron first-principles methods, will be presented in Sec. VI. Our qualitative model points to the main consequences of p-d repulsion in II-VI semiconductors.

(i) It reduces the direct band gap by repelling Γ_{15v} upwards without affecting the conduction-band minimum at Γ (of Γ_{1c} symmetry and, hence, non-pd). This was demonstrated also by Chang *et al.*,[21] who found a decrease by 1.2 eV in the calculated band gap of CdS when the Cd d band was included in the calculation. The better agreement with experiment for band gaps obtained using local-density-functional (LDF) calculations which neglect p-d repulsion is hence fortuitous. A particularly striking example is provided by the fact that despite the greater ionicity of ZnO, it has a *smaller* band gap [~ 3.4 eV (Ref. 37) in its wurtzite form] than ZnS: 3.90 to 3.82 eV for wurtzite and zinc-blende forms, respectively.[39] (Cd and Hg oxides also have smaller direct band gaps relative to their sulfides; however, the situation there is complicated by different crystal structures. This is contrary to the situation encountered in salts which lack active d bands, e.g., the more ionic compounds CaO, SrO, and BaO have *larger* band gaps (7.1, 5.3, and 4.4 eV, respectively[37]) than the corresponding less ionic sulfides CaS, SrS, and BaS (5.8, 4.8, and 3.9 eV, respectively[37]). We suggest that the reason for this is the stronger p-d repulsion in ZnO [where the Zn $3d$ to O $2p$ orbital energy difference is small; see Fig. 6(b) below] relative to ZnS (having a larger Zn $3d$ to S $3p$ orbital energy difference).

Again, empirical adjustment of the band-structure parameters can be used to reproduce the experimental band gap even if the d bands are ignored.[15(c)] However, the physical mechanism leading to these trends remain obscure in such approaches.

(ii) Since p-d repulsion raises the energy of the valence-band maximum, E_v, in inverse proportion to the (anion p)-(cation d) energy difference [Eq. (5)], a pair of materials AC and BC having a common anion C but whose cations A and B have different d-orbital energies (e.g., CdTe and HgTe, see Fig. 1 and Tables I and III) and wave functions would also have different values of ΔE_{pd}. The difference $\delta_{pd}=\Delta E_{pd}(AC)-\Delta E_{pd}(BC)$ will hence contribute to the valence-band discontinuity between AC and BC (see Tables VI and VIII). Whereas models which neglect the cation d band[54,55] have largely failed in predicting the substantial valence-band discontinuity[54,55] in, e.g., CdTe/HgTe, inclusion of d bands produces the correct results.[56] This will be further discussed in Sec. VI E.

(iii) p-d coupling mixes d character into the wave function at the valence-band maximum. (This is verified by direct calculations, see Sec. VI B.) Since d states contribute with opposite sign to the spin-orbit splitting (lowering

TABLE VI. Calculated relative shifts $\delta_{pd}=\Delta E_{pd}(AC)-\Delta E_{pd}(BC)$ (in eV) of the valence-band-maximum energy between two compounds AC and BC due to p-d repulsion from Table V (model A). This shift contributes directly to the valence-band offset between AC and BC (see Appendix). The models A1, A2, and A3 refer to Table V and the Appendix.

	CdTe/ZnTe	ZnTe/HgTe	CdTe/HgTe
Model A1	−0.10	0.43	0.33
Model A2	−0.06	0.33	0.27
Model A3	−0.02	0.33	0.31

TABLE VII. Calculated p-d-repulsion energies ΔE_{pd} [Eq. (5)] for ZnTe, CdTe, and HgTe (in eV), using model B of the Appendix, where bandwidths are used to determine ΔE_{pd}. For the input atomic eigenvalues, see Table III. We use experimental lattice parameters (see Table II). The "old" parameters [Ref. 22(a)] in Harrison's TB model (model B1) are $V_{pp}=2.16\hbar^2/md^2$ and $V_{ss}=-5.60\hbar^2/md^2$. The more recent parameters [Ref. 49(b)] (model B2) are $V_{pp}=1.28\hbar^2/md^2$ and $V_{ss}=-5.28\hbar^2/md^2$, where $d=(\sqrt{3}/4)a$ is the bond length. Here, $W_{\rm tot}$ is the total valence-band width (Γ_{15v} to Γ_{1v}) as obtained in tight-binding ($W_{\rm tot}^{\rm TB}$) calculations neglecting p-d repulsion, or in the present work ($W_{\rm tot}$), where p-d repulsion is included. See Appendix for details.

	ZnTe			CdTe			HgTe		
	$W_{\rm tot}^{\rm TB}$	$W_{\rm tot}$	ΔE_{pd}	$W_{\rm tot}^{\rm TB}$	$W_{\rm tot}$	ΔE_{pd}	$W_{\rm tot}^{\rm TB}$	$W_{\rm tot}$	ΔE_{pd}
Model B1	11.36	11.91	0.55	10.94	11.30	0.36	11.17	12.03	0.86
Model B2	11.67	11.91	0.24	11.20	11.30	0.10	11.40	12.03	0.63

it), as opposed to p orbitals (which raise it), p-d coupling would hence affect the trends in spin-orbit energies. This will be discussed in Sec. VI C.

(iv) Depending on whether the cation d-orbital energy is below the anion p energy [as depicted in Fig. 4(b)] or above it, the order of the e and t_2 cation d levels could change. Figure 5 depicts the two possibilities, both for O_h^5 [Figs. 5(a) and 5(b)] and T_d^2 [Figs. 5(c) and 5(d)] symmetries. Electrostatic (point-ion) crystal-field models[42] predict universally a level ordering of t_2 below e for O_h^5 symmetry, and e-below t_2 for T_d^2 symmetry. In O_h^5 symmetry, no p-d coupling exists and, hence, $\Gamma_{25'}(d)=t_2$ is predicted to be [Figs. 5(a), and 5(b)] lower in energy than $\Gamma_{12}(d)=e$, by crystal-field theory.[42] [Indeed, virtually all rocksalt-structure $3d$ oxides have the order depicted in Fig. 5(b); see Ref. 57.] In T_d^2 symmetry, on the other hand, we find either the normal level ordering [Fig. 5(d)] or an inverted order [Fig. 5(c)], depending on the order of the *atomic* anion p and cation d levels: inspection of the calculated atomic-orbital energies of the elements forming I-VII, II-VI, and III-V compounds (Fig. 6) shows cases of d-above-p ordering: CuCl, CuBr, CuI, AgF [Fig. 6(a)], spin-down Mn states in Mn chalogenides [Fig. 6(b)], or the unoccupied Al $3d$ states in Al$X^{\rm V}$ compounds (not shown). The pertinent p-d-coupling scheme is depicted in Fig. 5(d) and predicts that the two states showing strong cation d character, $t_2=\Gamma_{15}(dp)$ and $e=\Gamma_{12}(d)$, will occur in the normal order, e below t_2. This is indeed confirmed by band-structure calculations of Cu halides[58,59] and MnTe.[11] The fact that the VBM in Cu$X^{\rm VII}$ is a Cu d-like $\Gamma_{15}(dp)$ state (whereas the CBM is Cu s-like) is also consistent with the observation that the Γ_{15v}-Γ_{1c} band gap depends only weakly on $X^{\rm VII}$: it is[39] 3.3, 3.0, and 3.05 for CuCl, CuBr, and CuI, respectively. In contrast, in all II-VI [Fig. 6(b)] and III-V [Fig. 6(c)] compounds one expects the occupied cation d state to lie *below* the anion p state. Here, the pertinent p-d-coupling scheme is given in Fig. 5(c), predicting that the two states showing strong d character [$t_2=\Gamma_{15}(dp)$ and $e=\Gamma_{12}(d)$] will occur in reverse order, (i.e., t_2 below e) relative to Fig. 5(d) or the predictions of crystal-field theory. Indeed, band-structure calculations[4-11] for II-VI and III-V compounds (e.g., see Figs. 2 and 3 for the former) exhibit this inverted order [this is also the case for γ-AgI, see Fig. 6(a) and Ref. 59]. This puzzling conflict between point-ion crystal-field models and band-structure calculations for II-VI compounds in zinc-blende structure is resolved by acknowledging p-d repulsion.

TABLE VIII. Calculated relative shifts $\delta_{pd}=\Delta E_{pd}(AC)-\Delta E_{pd}(BC)$ (in eV) of the valence-band-maximum energy between two compounds AC and BC due to p-d repulsion, using the data of Table VII ("model B"). Models B1 and B2 refer to Table VII and the Appendix.

	CdTe/ZnTe	ZnTe/HgTe	CdTe/HgTe
Model B1	0.19	0.31	0.50
Model B2	0.14	0.39	0.53

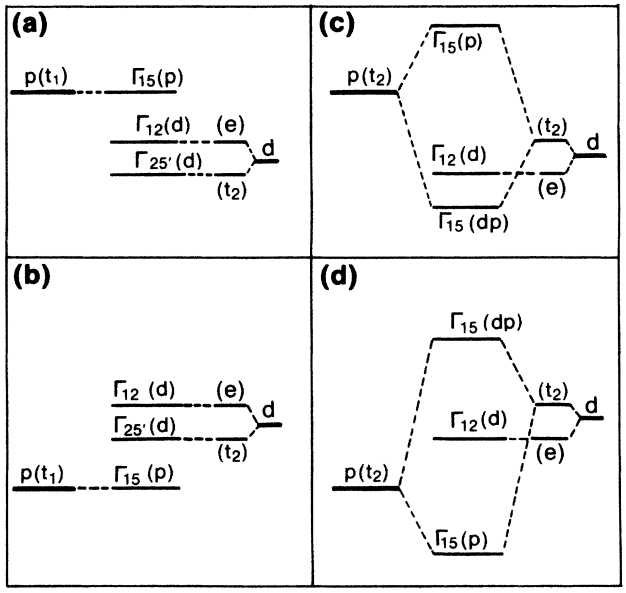

FIG. 5. Schematic plot of energy-level–interaction scheme of anion p and cation d states in O_h^5 [parts (a) and (b)] and T_d^2 [parts (c) and (d)] symmetries. (a) and (c) $\varepsilon_p>\varepsilon_d$; (b) and (d) $\varepsilon_p<\varepsilon_d$. Notice that in O_h^5 symmetry [(a) and (b)] pd hybridization is symmetry forbidden. In (c) the order of cation-d t_2 and e states is reversed due to p-d repulsion.

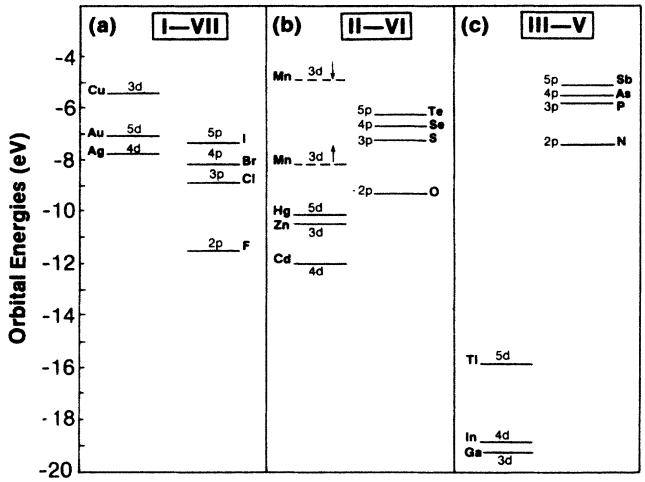

FIG. 6. Calculated LDF free-atom orbital energies of cation *d* and anion *p* states pertinent to (a) I-VII, (b) II-VI, and (c) III-V compounds.

(v) Whereas *p-d* repulsion conserves the center of gravity of the unperturbed states (hence, since both are occupied, the sum of their orbital energies is conserved so the first-order correction to the cohesive energy vanishes), this repulsion alters the nature of the wave functions of valence states through admixture of antibonding character into the upper valence states. This *p-d*-induced change in the wave function then leads to a second-order correction to the total energy of the solid. As *antibonding* character is mixed into the upper valence bands, it could lead to a destabilization of the lattice, e.g., to smaller cohesive energies and larger lattice parameters relative to cases where *p-d* repulsion is absent. This will be examined quantitatively in Sec. VI A, where we find that *p-d* repulsion depletes charge from the anion-cation bond, hence substantially reducing (e.g., by 58% in HgTe) the cohesive energy and increasing (by 13%) the lattice parameter.

IV. OTHER EVIDENCE

There are other known phenomena which manifest unusual behavior due to *p-d* coupling in tetrahedral semiconductors which we briefly review.

A. Why are Cu acceptor states anomalously deep in II-VI semiconductors?

The standard technique for producing low-resistivity *p*-type semiconductors is to dope them with impurity atoms positioned in the periodic table to the left of the cation atom. Such is the case for *Ga*As:Zn, Si:B, Ge:Al, etc., all exhibiting *shallow* acceptor states at about 0.1 eV or less from the valence-band maximum. However, using the same principle for II-VI materials (e.g., doping with Cu) has, surprisingly produced *deep* substitutional acceptor states, e.g.,[39,60] at $>E_v+1.2$ eV, $E_v+0.75$ eV, and $E_v+0.15$ eV for Cu in ZnS, ZnSe, and ZnTe, respectively, leading to insulating behavior in the first two cases. Similar values, decreasing as the anion changes from S to Se and Te, have also been obtained in Cd-based II-VI compounds:[39] the Cu acceptor levels are at $E_v+1.19$ eV, $E_v+0.64$ eV, and $E_v+0.39$ eV for CdS, CdSe, and CdTe, respectively.[39]

These phenomena are naturally explained[61] in terms of *p-d* repulsion between the Cu^{2+} 3*d* orbitals and the S, Se, and Te *p* orbitals. The small Cu^{2+} *d* to anion *p*-orbital energy separation [$\varepsilon_p^a-\varepsilon_d^c$ of Eq. (5)] leads to a substantial repulsion to higher energies of the antibonding states, constituting in this case the impurity acceptor level [Fig. 4(b)]. This repulsion is similar in CdX^{VI}:Cu^{2+} or ZnX^{VI}:Cu^{2+} (since the nearest-neighbor environment around the cation-replacing Cu atom is identical), but diminishes as the anion X^{VI} orbitals are further removed in energy from the Cu^{2+} *d* orbitals, i.e., in the sequence S→Se→Te [observe in Tables II and IV the increase in the energy denominator $\varepsilon_p^a-\varepsilon_d^c$ of Eq. (5) in this sequence]. In contrast, doping III-V compounds by Zn^{3+} leads to a very large energy separation between Zn^{3+} 3*d* and the *p* orbitals of P, As, or Sb [Fig. 6(c) and Table IV]; hence, according to Eq. (5) the *p-d* repulsion is smaller and the resulting acceptor states are shallower relative to Cu in II-VI's. If one dopes II-VI compounds by monovalent atoms lacking active *d* orbitals (e.g., Li and Na), one finds *shallow* acceptor states (at[39,60] $E_v+0.1$ eV for *Zn*Se:Na, $E_v+0.06$ eV for *Zn*Te:Li, $E_v+0.17$ eV for *Cd*S:Na, and $\sim E_v+0.1$ eV for *Cd*Se:Na) since no *p-d* repulsion exists (here, the situation is, however, complicated by the formation of interstitial donor impurities in addition to the substitutional impurities, leading to electrical compensation[60]).

B. Anomalously small band baps and spin-orbit splitting in tetrahedral chalcopyrites

The tetrahedrally bonded *IB*-III-VI_2 chalcopyrites[62] (e.g., $CuGaSe_2$) resemble structurally the zinc-blende form of the II*B*-VI compounds, yet their band gaps are enormously smaller than those of the corresponding binary chalcogenides, e.g.,[61] $E_g(CuGaS_2)=2.43$ eV, $E_g(CuGaSe_2)=1.68$ eV, and $E_g(CuGaTe_2)=1.23\pm0.1$ eV, compared with[37] $E_g(ZnS)=3.82$ eV, $E_g(ZnSe)=2.87$ eV, and $E_g(ZnTe)=2.39$ eV, respectively. Had the valence-band maximum consisted of anion orbitals alone, one would expect roughly similar band gaps in $CuGaX_2^{VI}$ and ZnX^{VI}, since the average of Cu and Ga *s*-orbital energies (making up the conduction band in $CuGaX_2^{VI}$) is close to that of Zn. Instead, the band gaps of the $CuGaX_2^{VI}$ chalcopyrites are smaller by as much as 1.39, 1.19, and 1.16±0.1 eV relative to the analogous II-VI compounds for X^{VI}=S, Se, and Te, respectively.[61]

Again, the appropriate explanation seems to be the *p-d*-repulsion effect:[61] the Cu 3*d* orbitals in $CuGaX_2^{VI}$ are considerably closer in energy to the anion *p* orbitals than are the Zn 3*d* orbitals in ZnX^{VI} [Figs. 6(a) and 6(b)], leading to a far more effective *p-d* repulsion in the ternary chalcopyrites, with a consequent dramatic reduction in their band gaps (compounded by the fact that the Cu 3*d* orbitals are also more delocalized than the Zn 3*d* orbitals,

leading to a larger V_{pd} coupling matrix element in chalcopyrites and, hence, a larger *p-d* repulsion). Detailed band-structure calculations[61] have quantitatively demonstrated this effect by comparing the calculated band gaps with and without a chemically active Cu 3*d* band. They showed 25–33 % *d* character in the Γ_{15v} valence-band maximum of the chalcopyrites. This massive participation of *d* orbitals in the VBM also explains the anomalously low spin-orbit splitting observed in chalcopyrites:[62] (0.21, 0.23, 0.31, and 0.30 eV in $CuGaSe_2$, $CuInSe_3$, $AgGaSe_2$, and $AgInSe_2$, respectively, and nearly zero or negative in all sulfur-based chacogenides, compared with[39] ~0.45 eV in II-VI selenides, and <0.1 eV in II-VI sulfides). The opposite (negative) spin-orbit splitting contributed by *d* orbitals overwhelms much of the (positive) contribution due to anion *p* states. Simple estimates[62] showed that about 20–35 % *d* character at the VBM is needed to account for these reductions.

C. Inverted exchange splitting in MnTe

p-d repulsion in tetrahedral semiconductors leads to a particularly interesting new effect in the band structure of MnX^{VI} compounds. A curious coincidence (see Fig. 6) places the energies of the *p* orbitals of S, Se, and Te *between* the energies of spin-up and spin-down 3*d* orbitals of Mn. Extending the simple *p-d*–coupling model of Fig. 4 separately to spin-up and spin-down orbitals (Fig. 7) shows the following: the spin-up Mn 3*d* orbitals [denoted t_+ in tetrahedral symmetry, Fig. 7(a)] couple with the spin-up Te 5*p* orbitals [t_+ in Fig. 7(b)] to form a bonding (B_+) state and an antibonding (AB_+) state. Similarly, the spin-down Mn 3*d* orbitals [t_- in Fig. 7(a)] couple to the Te spin-down *p* orbitals [t_- in Fig. 7(b)] to give a bonding state B_- and an antibonding state AB_-. In the ground state of ferromagnetic MnTe, B_+, B_-, and AB_+ are occupied, and AB_- is empty. (Again, the *e* orbitals of Mn have no counterpart in Te and hence remain nonbonding.) The special coincidence of the atomic-orbital energies produces a large (positive) exchange splitting for the *dp* orbitals (the majority-spin state B_+ is lower in energy than the minority-spin state AB_-), but a smaller, and *negative* exchange splitting (minority-spin B_- below the majority-spin AB_+ state) for the hybridized *pd* states. This model predicts an unusual case where spin-polarized photoemission will show spin-up photoelectrons (from AB_+) at *lower* binding energies than spin-down photoelectrons (from B_-) for ferromagnetic Mn chalcogenides. Recent spin-polarized band-structure calculations for ferromagnetic (zinc-blende) MnTe and (CuAuI-like) $CdMnTe_2$ confirm this picture.[11] No experimental test exists to our knowledge.

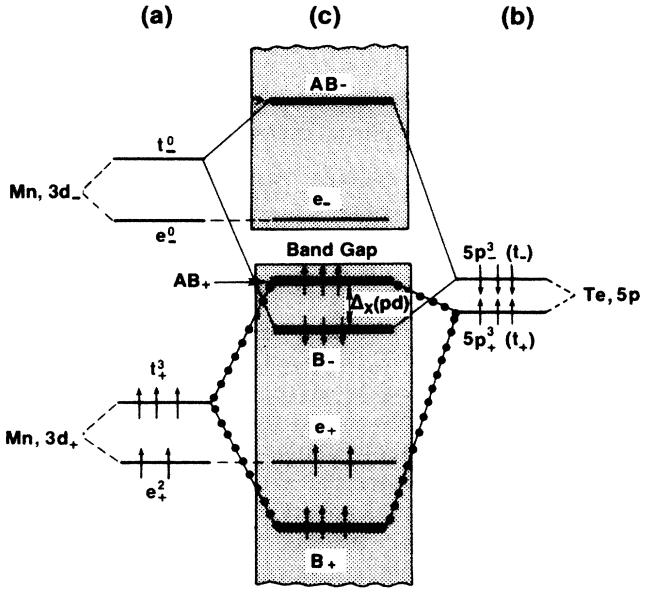

FIG. 7. Schematic diagram of the *p-d*–repulsion effects for the hypothetical ferromagnetic zinc-blende MnTe. (a) Exchange and crystal-field splitting of Mn 3*d* states, (b) exchange splitting of Te 5*p* states, and (c) the final interacting states. Shaded areas denote the host crystal bands. B_+ and B_- denote bonding states for spin up and spin down, respectively, whereas AB_+ and AB_- denote antibonding states for spin up and spin down, respectively. Note how *p-d* repulsion leads here to a negative *p-d* exchange splitting $\Delta_x(pd)$ (i.e., B_- is below AB_+).

V. METHOD OF CALCULATION

We have used the self-consistent first-principles, general potential, linearized-augmented-plane-wave (LAPW) method[63] within the local-density-functional formalism[64] to calculate the properties of ZnTe, CdTe, HgTe, and their ordered 50%-50% alloys. We used the Hedin-Lundqvist exchange-correlation formula.[51] The details of this method can be found elsewhere;[63] here we indicate features pertinent to the present study.

Since we are studying compounds with heavy-atom constituents, scalar-relativistic effects[65] (i.e., all relativistic effects except spin-orbit coupling) are included for all valence states (including the outermost cation *d* states). Core states are calculated fully relativistically using an atomiclike approach (i.e., retaining only the spherical part of the potential). No shape approximations are made on the crystal potential and charge density. All states (including the core states) are calculated fully self-consistently. In some instances [Sec. VI A and Table IX below], nonrelativistic and fully relativistic calculations have also been performed to separately study scalar-relativistic and spin-orbit effects. We include spin-orbit coupling through a second variational procedure.[66] We choose the muffin-tin radii R_{MT} to be $R_{MT}(Zn)=2.3532$ a.u., $R_{MT}(Te)=2.5137$ a.u., and $R_{MT}(Cd)=R_{MT}(Hg)=2.6742$ a.u. The cutoff energy for the basis functions is 11 Ry, equivalent to about 140 basis function per atom. Such a large cutoff energy is required because of the localized *d* orbitals and the requirement of nonoverlapping muffin-tin spheres for the LAPW method. The large lattice mismatch between ZnTe and (CdTe,HgTe) further prevents use of larger muffin-tin spheres (therefore a smaller cutoff energy) when studying ternary compounds. The nonspherical potential and charge density is expanded inside the muffin-tin spheres in terms of lattice harmonics up to $l=6$. All convergence parameters are kept

the same in calculations for the binary and ternary compounds in order to reduce random errors (which would otherwise produce slightly different total energies per atom of the same compound calculated in, say, a zinc-blende or in a double-zinc-blende unit cell).

The Brillouin-zone (BZ) integration for the charge density and total energy is performed using a discrete **k**-point summation. The special **k**-point scheme of Chadi and Cohen[67] for the zinc-blende structure and their equivalent[68] **k** point scheme for the CuAuI and the Cu_3Au-like structures are used. This equivalent **k**-point procedure is necessary in comparing the extremely small energy differences between the ternary compounds and their binary constituents. A uniformly distributed eight-**k**-point sampling in the face-centered-cubic BZ has also been tested. This test is needed since HgTe is a zero-gap semimetal with an inverted band *at the* Γ *point* [Fig. 2(c)]: inclusion of the Γ point in this eight-**k**-point sampling scheme is then used to examine the sensitivity of the ground-state properties with respect to the **k**-point sampling. We find that relative to the two-special-**k**-point sampling the values obtained with eight **k**-point calculations are similar to those obtained with the 10 special[67] **k** points. The latter sampling produces somewhat smaller lattice constants ($\sim$0.02 Å) and smaller bulk moduli ($\sim$10%) for all three compounds we studied.

VI. RESULTS

A. Ground-state properties

1. *All-electron results: Relativistic effects*

Table IX compares ground-state properties of ZnTe, CdTe, and HgTe (equilibrium lattice parameters, cohesive energies, and bulk moduli) calculated using different all-electron techniques[69,70] [the present LAPW as well as the linear muffin-tin orbitals (LMTO) methods], all retaining the cation *d* bands. The agreement in the results obtained by these different techniques is rather good. Note, in particular, the effect of relativistic corrections: Comparing nonrelativistic (NR) with semirelativistic (SR) calculations, one notices for the latter case that both the equilibrium lattice parameters and the cohesive energies are reduced relative to the nonrelativistic limit. The qualitative reason for this can be appreciated from the relativistic shift in the *atomic*-orbital energies (Table III). While in nonrelativistic atomic calculations Cd and Hg have similar *s*- and *p*-orbital energies (hence, one would expect the normal trend that the compound with heavier atoms—Hg—would have a larger lattice constant than the compound with a lighter atom), relativistic effects contract the *s* orbitals, making them more localized and more tightly bound (by 0.16, 0.39, and 1.54 eV for Zn 4*s*, Cd 5*s*, and Hg 6*s*, respectively). This reduces their direct contribution to the cohesive energy, as both the ionization of these electrons (required to form ionic bonds) and their promotion to *p* orbitals (required to form covalent bonds) become more energetically costly. Since the relativistic contraction of the *s* orbitals reduces the effective atomic sizes, it also reduces the equilibrium lattice parameters (compare nonrelativistic and semirelativistic lattice parameters of HgTe in Table IX). This contraction of *s* orbitals better shields the nucleus, presenting the non-*s* orbitals with a less attractive (better screened) interaction with the atomic core. Consequently, the *increased* binding of the *s* orbitals is associated with a *decrease* in the binding of non-*s* electrons (e.g., by 0.41, 0.89, and 2.28 eV for Zn 3*d*, Cd 4*d*, and Hg 5*d*, respectively). As the outer *d* electrons become shallower, they approach more closely the energies of the anion *p* states (which are less affected by relativistic effects; see Table III). According to Eq. (5), this enhances the *p-d* repulsion, which further reduces the cohesive energies.

Comparing the semirelativistic with the fully relativistic calculations for HgTe (Table IX), we see that spin-orbit effects (present in the calculations labeled R but missing from those labeled SR) make only a small contribution to the ground-state properties. This manifests the fact that spin-orbit splittings do not substantially change the bonding-antibonding character of the wave functions, and that the larger splitting at the valence-band maximum (which is uncompensated in HgTe due to the reversed band structure) contributes little to the overall Brillouin-zone integral involved in calculating the total energy. Our results hence do not support the substantial (0.08 Å) spin-orbit-induced reduction of the lattice constant predicted by Cade and Lee.[70]

2. *Effects of p-d repulsion on ground-state properties*

To qualitatively assess the effect of *p-d* repulsion on the ground-state properties, we compare in Table X the re-

TABLE IX. Comparison of calculated equilibrium lattice parameters (a, in Å), cohesive energies E_c [in eV/(atom pair)], and bulk moduli B (in GPa), as obtained by all-electron–calculation techniques, using nonrelativistic (NR), semirelativistic (SR), and fully relativistic (R) density-functional theory. Exchange-correlation functional of Ref. 51 is used.

	ZnTe			CdTe				HgTe				
Property	LAPW[a] NR	LAPW[a] SR	LMTO[b] SR	LAPW[a] NR	LAPW[a] SR	LMTO[b] SR	LMTO[c] SR	LAPW[a] NR	LAPW[a] SR	LAPW[a] R	LMTO[c] R	LMTO[c] SR
a (Å)	6.093	6.052	6.174	6.541	6.470	6.545	6.45	6.656	6.492	6.490	6.49	6.57
E_c (eV/pair)	5.93	5.64		5.62	5.35			5.32	4.46	4.57		
B (GPa)	56.9	52.1	51.2	44.7	44.0	46.8	59.0	41.6	46.1	45.6	52.5	42.8

[a]Present results, using a single energy panel.
[b]Reference 69, using a single energy parameter for the muffin-tin orbitals. Two-panel calculation gives similar results.
[c]Reference 70, using two energy panels.

TABLE X. Comparison of calculated ground-state properties of II-VI compounds (lattice parameter a, cohesive energy E_c, and bulk modulus B) using the present all-electron (LAPW) approach, which retains the cation d band, and a pseudopotential (ps) approach, which does not. Both calculations are semirelativistic. Experimental results are given for comparison.

	ZnTe			CdTe			HgTe		
Property	With d (LAPW)[a]	Expt.	No d (ps)[b]	With d (LAPW)[a]	Expt.	No d (ps)[b]	With d (LAPW)[a]	Expt.	No d (ps)[b]
a (Å)	6.052	6.089[c]	5.618	6.470	6.481[d]	5.818	6.492	6.461[e]	5.616
E_c (eV/pair)	5.64	4.82[f]	6.75	5.35	4.45[f]	6.77	4.46	3.22[f]	7.05
B (GPa)	52.1	50.9[g]	27.3	44.0	44.5[h]	13.3	46.1	47.6[h]	4.7

[a]Present results.
[b]Pseudopotential study of Ref. 20 in which the cation d band is frozen. This calculation, like the one reported here, uses the Hedin-Lundqvist exchange-correlation functional.
[c]Reference 71.
[d]Reference 72.
[e]Reference 73.
[f]References 35 and 36; also see Table II.
[g]Reference 74.
[h]Reference 75.

sults obtained here (retaining the cation d bands) with those obtained using the first-principles pseudopotential method[20] [assuming frozen $(n-1)d$ cation orbitals; hence, without a cation d band]. The latter method incorporates the indirect effects of the d orbitals on the atomic valence s and p pseudopotentials but lacks d-band *wave functions* in the solid, hence missing the p-d-repulsion effect. Comparison of the calculated ground-state properties with experiment[35–36,71–75] (Table X) shows rather good agreement when cation d bands are retained (present results), but demonstrates that when the cation d bands are omitted (pseudopotential results,[20] denoted in Table X as "no d") the predicted equilibrium lattice constants a_{eq} are too small relative to experiment by 7.7%, 10.2%, and 13%, and the predicted bulk moduli are too small by 46%, 70%, and 90% for ZnTe, CdTe, and HgTe, respectively. [Note that whereas adding ten protons and ten d electrons to a IIA-VI compound *reduces* the lattice parameter (Table II), inclusion of an active d band in IIB-VI compounds (Table X) *increases* the lattice parameters.] The underlying local-density formalism itself is not free of error; for example, we find a_{eq} of HgTe to be larger than a_{eq} of CdTe by 0.022 Å, while the experimental result[72,73] shows a_{eq}(HgTe) to be smaller than a_{eq}(CdTe) by 0.02 Å. A similar trend is apparent in the LMTO results[70] and in our calculation[68] for the face-centered-cubic (fcc) noble metals, showing a_{eq} for fcc Au to be slightly larger than a_{eq} for Ag, whereas the experimental result shows Au to have a slightly smaller lattice parameter than Ag. Such errors in a_{eq}, of order 0.5%, are not surprising since the outer d orbitals are somewhat too shallow and consequently too extended in LDF theory, causing an overestimation of the overlap repulsion. Similarly, our calculated cohesive energies are too large by 1–1.5 eV, a consequence of neglecting multiplet-stabilization energies (more negative in the free atoms than in the solids and decreasing along the Zn→Cd→Hg sequence).[76] However, the discrepancies relative to experiment evident in the "no d" pseudopotential calculation far exceed the error limits of the local-density method or intrinsic convergence errors. They are particularly large for HgTe, which has the shallowest (and most spatially delocalized) cation d orbitals (Tables I and III). Although such systematic discrepancies can be fixed by adding an empirical repulsive potential term, adjusted to fit the experimental ground-state properties,[20] the need for such substantial adjustments in models which omit d bands testifies to the significant role of p-d repulsions in destabilizing these systems. On the other hand, direct-overlap interaction between the anion sp orbitals and the cation d orbitals can increase the cohesive energy of the II-VI system,[11] relative to systems which have less active d orbitals (e.g.,[11] MnTe relative to CdTe). This direct-overlap interaction hence acts in the opposite direction to the p-d repulsion. This is the main reason why transition-metal compounds (which have chemically active, open-shell d orbitals) have large cohesive energies.[11] Since Hg has rather delocalized d orbitals, the neglect of d bands in the tight-binding calculation could underestimate[77,78] the cohesive energies of HgTe.

Calculations of alloy phase diagrams often require knowledge of the relative cohesive energies ΔH of an ordered ternary phase[68] (e.g., $CdHgTe_2$) with respect to equivalent amounts of the binary constituents (e.g., CdTe + HgTe). It is interesting to note that calculation techniques which omit p-d repulsion have predicted overly negative formation enthalpies, e.g., $\Delta H=-0.6$ meV/(4 atoms) using tight-binding,[79] or $\Delta H=-60$ meV/(4 atoms) using pseudopotentials[20] for $CdHgTe_2$ in the CuAuI-like structure, compared with the present result of $\Delta H=+12.3$ meV/(4 atoms). Although the small magnitude of these energies and the numerical intricacies involved in obtaining them make it difficult to quantitatively assess their precision, our foregoing discussion suggests that here, too, omission of the destabilizing p-d repulsion could be responsible for the predicted stability of the ordered phase in both tight-binding and pseudopotential methods, compared with the instability predicted here (no compoundlike ordering of $CdHgTe_2$ is found experimentally).

TABLE XI. Band energies (in eV, relative to the valence-band maximum) and percentage of *s*, *p*, and *d* character in the muffin-tin spheres. The percentage of the total *s*, *p*, and *d* charge of a state enclosed in the sphere ("tot spheres") is given too. State labels are given both for semirelativistic (SR) and relativistic (R) cases. First line for anion, second for cation. The muffin-tin radii are $R_{MT}(Zn)=2.3532$, $R_{MT}(Te)=2.5137$, and $R_{MT}(Cd)=R_{MT}(Hg)=2.6742$, all in a.u.

		ZnTe					CdTe					HgTe				
State Label						tot					tot					tot
SR	R	ε (eV)	*s* (%)	*p* (%)	*d* (%)	spheres (%)	ε (eV)	*s* (%)	*p* (%)	*d* (%)	spheres (%)	ε (eV)	*s* (%)	*p* (%)	*d* (%)	spheres (%)
Γ_{1v}	Γ_6	−11.91	58.9	0	0	68.4	−11.30	61.6	0	0	70.6	−12.03	59.5	0	0	70.5
			9.5	0	0			9.0	0	0			11.0	0	0	
Γ_{15d}	Γ_8,Γ_7	−7.27	0	2.5	0.1	96.0	−8.43	0	2.4	0.1	95.2	−7.38	0	5.5	0.2	90.8
			0	0.1	93.3			0	0.1	92.6			0	0.1	85.0	
Γ_{12d}	Γ_8	−7.05	0	0	0.2	97.4	−8.17	0	0	0.2	96.6	−6.87	0	0	0.3	93.9
			0	0	97.2			0	0	96.4			0	0	93.6	
Γ_{15v}	Γ_7,Γ_8	0	0	57.3	0.2	69.0	0	0	55.8	0.1	67.3	0	0	53.8	0	70.7
			0	4.3	7.2			0	4.0	7.4			0	4.0	12.9	
Γ_{1c}	Γ_6	1.02	28.2	0	0	65.7	0.47	24.2	0	0	62.0	−0.99	25.5	0	0	70.8
			37.5	0	0			37.8	0	0			45.3	0	0	
Γ_{15c}	Γ_7,Γ_8	4.32	0	1.6	10.6	42.8	4.48	0	1.0	9.2	43.5	4.17	0	1.0	9.7	42.3
			0	30.4	0.2			0	33.2	0.1			0	31.5	0.1	
X_{1v}	X_6	−10.73	69.1	0	0	78.2	−10.79	61.6	0	0	79.6	−11.27	66.7	0	0	78.4
			0	2.7	6.4			0	2.2	15.8			0	2.4	9.3	
X_{3v}	X_7	−5.13	0	23.5	1.0	60.6	−4.44	0	24.3	0.6	60.0	−5.50	0	15.7	1.0	68.5
			29.6	0	6.5			32.3	0	2.8			37.7	0	15.1	
X_{5v}	X_6,X_7	−2.21	0	42.6	0	55.9	−1.92	0	42.1	0	55.7	−2.27	0	40.9	0	56.1
			0	11.6	1.7			0	12.0	1.6			0	11.3	3.9	
X_{1c}	X_6	2.25	5.5	0	5.6	25.7	2.45	5.1	0	4.2	26.5	2.35	5.9	0	4.1	28.8
			0	11.3	3.3			0	13.8	3.4			21.9	0	6.0	
X_{3c}	X_7	2.15	0	10.4	7.3	43.0	2.54	0	12.0	5.7	45.8	1.80	0	19.3	4.3	51.5
			22.0	0	3.3			24.6	0	3.5			21.9	0	6.0	
L_{1v}	L_6	−11.04	66.3	0	0	75.4	−10.91	62.1	0	0	77.4	−11.47	64.7	0	0	76.1
			3.2	1.8	4.1			2.4	1.7	11.2			3.4	1.6	6.4	
L_{1v}	L_6	−5.27	1.1	26.6	0.3	51.6	−4.54	0.8	25.9	0.2	52.8	−5.54	2.8	21.7	0.2	57.1
			19.8	3.7	0.1			22.0	3.9	0			26.8	3.5	2.1	
L_{3v}	$L_6,L_{4,5}$	−0.92	0	50.0	0.3	64.1	−0.80	0	49.1	0.2	62.9	−0.99	0	46.8	0.2	64.6
			0	9.3	4.5			0	9.1	4.5			0	9.1	8.5	
L_{1c}	L_6	1.61	11.4	4.6	4.2	53.3	1.60	10.0	5.1	3.1	52.8	0.54	9.8	10.0	2.4	55.9
			28.4	3.5	1.2			29.2	4.5	0.9			27.5	4.6	1.6	

B. Antibonding *d* character in the upper valence bands

Figure 2 depicts the calculated band structures of ZnTe, CdTe, and HgTe, and Table XI gives the band energies at high-symmetry points in the Brillouin zone, together with the percentage of *s*, *p*, and *d* character inside the muffin-tin sphere for each atom. Since not all of the amplitude of a given state is enclosed in such spheres, Table XI also gives, for each state, the percentage of charge enclosed inside all atomic spheres.

Inspection of the orbital character of the various band states in ZnTe, CdTe, and HgTe (Table XI) reveals a number of interesting features: (i) states that can mix *d* character by symmetry do so. This is evident at the valence-band maximum Γ_{15v} (7.2%, 7.4%, and 12.9% cation *d* character in ZnTe, CdTe, and HgTe, respectively), in Γ_{15c} (10.6%, 9.2%, and 9.7% anion *d* character in ZnTe, CdTe, and HgTe, respectively), and in X_{3v} (6.5%, 2.8%, and 15.1% cation *d* character in ZnTe, CdTe, and HgTe, respectively). Note that the distinguishing feature of the Γ_{15v} state in ZnTe, CdTe, and HgTe is not the extent of cation *p* character (these three compounds all have $\sim 4\%$ cation *p* character), but the difference proportions of cation *d* character. (ii) States forming the anion *s* band at the bottom of the valence band (e.g., X_{1v} and L_{1v}) also include contributions from the cation *d* states: 6.4%, 15.8%, and 9.3% in X_{1v}, and 4.1%, 11.2%, and 6.4% in L_{1v}, for ZnTe, CdTe, and HgTe, respectively. This suggests that the photoemission peak corresponding to the anion *s* band (indicated in Fig. 1 by an arrow near ~ -12 eV) could exhibit a contribution (e.g., a low-energy shoulder in ZnTe and CdTe) due to the tailing density of states of the cation *d* band. This effect is absent in the photoemission spectra of III-V compounds lacking a *d* band (e.g., BP and AlP). Furthermore, since the L_{1v} and X_{1v} states contain *d* character, but the Γ_{1v} does not (by symmetry), *p-d* repulsion acts to *narrow* the lowest, L_{1v}-Γ_{1v}-X_{1v} valence band (while broadening the upper L_{1v}-Γ_{15v}-X_{3v} valence band). (iii) The conduction-band minimum at Γ_{1c}, described by tight-binding methods[22–26] as a *cation s* states, has significant *anion*[5] character as well, e.g., 28.2% 24.2%, and 25.5% for ZnTe, CdTe, and HgTe, respectively.

Table XII compares the calculated band gaps, *d*-band energies, and spin-orbit splittings at Γ and L with the observed values.[80–86] Calculated band gaps and *d*-band binding energies show the expected underestimation relative to experiment, both phenomena characteristic of the local-density-functional theory. The occurrence of the metal *d* band inside the upper valence band, its non-negligible dispersion, and the direct appearance of *d* character in the upper valence band testify to the chemically active nature of *d* bands in these materials.

The simple tight-binding argument for *p-d* mixing described in Sec. III and Fig. 4(b) suggests the antibonding character in the valence-band-maximum state Γ_{15v} to be the hallmark of *p-d* mixing. Figure 8(a) depicts the calculated wave function squared for the Γ_{15v} state in HgTe, clearly exhibiting a minimum along the Hg—Te bond direction (partially a consequence of the ionicity of this bond) and characteristic *antibonding lobes* around the Hg site (i.e., pointing *away* from the nearest bonded atoms, towards the interstitial sites). These antibonding lobes are absent in the Γ_{15v} state of semiconductors which lack any significant *p-d* repulsion (e.g., III-V compounds). Similar antibonding features are exhibited, e.g., by the L_{3v} state [Fig. 8(b)] and the X_{5v} state [Fig. 8(c)], all absent in the analogous states in III-V compounds. An even stronger *p-d* mixing character is exhibited by the Γ_{15v} state of ferromagnetic zinc-blende MnTe (Fig. 9):

TABLE XII. Calculated band gaps (E_g, in eV), center of *d*-band energies ε_d, spin-orbit splittings of valence bands at $\Gamma(\Delta_0)$ and $L(\Delta_1)$, and that of the cation *d* bands, Δ_d, for ZnTe, CdTe, and HgTe.

	ZnTe			CdTe			HgTe		
	LMTO[a]	LAPW[b]	Expt.	LMTO	LAPW[b]	Expt.	LMTO[c]	LAPW[b]	Expt.
E_g(NR)		1.98			1.44			1.14	
E_g(SR)	0.96	1.02		0.51[a]	0.47			−0.99	
E_g(R)	0.63	0.72	2.39[d]	0.29[a] 0.47[c]	0.18	1.59[e]	−1.06	−1.27	−0.30[f]
ε_d	−7.2	−7.18	−9.84[g]	−8.55[a] −7.80[c]	−8.33	−10.49[g]	−7.38	−7.18	−8.58[g]
Δ_0	1.01	0.89	0.91[h]	0.90[a] 0.95[c]	0.86	0.90[i]	0.90	0.78	1.08[j]
Δ_1	0.58	0.51	0.53[k]	0.55[a] 0.57[c]	0.53	0.54[k]	1.31[l]	0.53	0.62[k]
$-\Delta_d$		0.37	0.3[m]	0.5[c]	0.69	0.63[m]	1.7	1.68	1.85[m]

[a]See Ref. 69 for details.
[b]Present results.
[c]Reference 70.
[d]Reference 80.
[e]Reference 81.
[f]Reference 82.
[g]Reference 2.
[h]Reference 83.
[i]Reference 84.
[j]Reference 85.
[k]Reference 86.
[l]Reference 70; this could be a printing error.
[m]Reference 1.

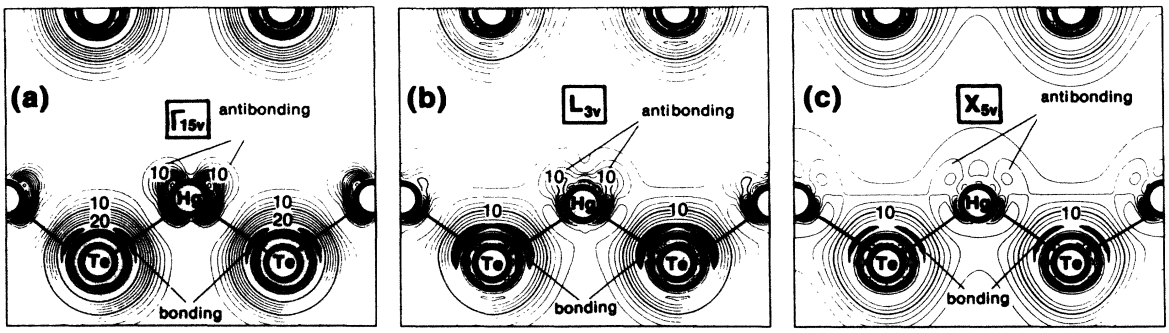

FIG. 8. Wave-function amplitudes for HgTe valence-band states at some high-symmetry points (normalized to two electrons per unit cell). (a) Γ_{15v} state, (b) L_{3v} state, and (c) X_{5v} state. The charge density is given in units of 10^{-3} e/a.u.^{3}; the step size is 2. Antibonding and bonding features are indicated.

the spin-up Te 5*p* orbital [Fig. 9(a)] forms a strong *antibonding* combination with the corresponding spin-up orbital of Mn 3*d* leading to a node along the Mn—Te bond, whereas the spin-down Te 5*p* orbital forms a *bonding* combination [Fig. 9(b)] with the corresponding Mn 3*d* orbital (also see Fig. 7). The antibonding character mixed into the valence-band maximum in II-VI compounds reflects the constraint of orthogonality to the corresponding Γ_{15} state of the metal *d* band [$\Gamma_{15}(dp)$ in Fig. 4]. This is demonstrated in Fig. 10(a), which depicts the charge density contributed by this $\Gamma_{15}(dp)$ state, showing its *bonding* charge buildup, oriented *along* the Hg—Te bond. [Note that the Γ_{12d} state, depicted in Fig. 10(b), is nonbonding, with its atomiclike charge distribution.]

To isolate directly the effect of *p-d* repulsion on the ground-state charge density, we have repeated band-structure calculations for CdTe and HgTe, where the cation *d* orbitals are effectively removed from the basis set. (This was done by setting the LAPW energy parameters[63] $E_{l=2}^{\mathrm{Cd}}$ and $E_{l=2}^{\mathrm{Hg}}$ for the *d*-wave basis functions inside the Cd and Hg spheres to values which are distant from the corresponding *d*-band energies.) We then plot the resulting total valence-band charge densities from the valence-band maximum Γ_{15v} to the valence-band minimum Γ_{1v}, omitting, however, the contribution of the cation *d* band itself (which does not exist in this artificial calculation) in Figs. 11(a) (for HgTe) and 11(b) (for CdTe). The corresponding valence charge densities of HgTe and CdTe calculated with *p-d* repulsions (i.e., retaining the cation *d* band in the variational calculations) is shown for CdTe

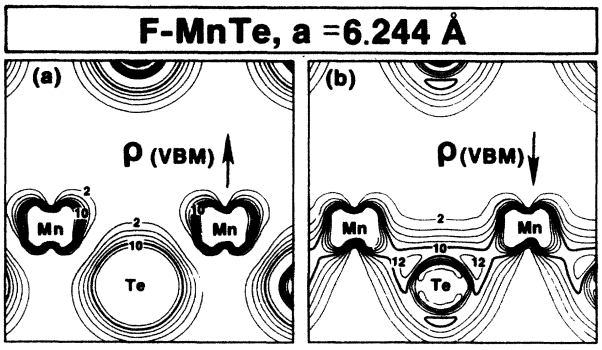

FIG. 9. Same as Fig. 9, but for ferromagnetic zinc-blende MnTe. (a) Spin-up valence-band-maximum state and (b) spin-down valence-band-maximum state. Note the antibonding character in (a) (node along Mn—Te bond) and the bonding character in (b). See caption to Fig. 8 for units.

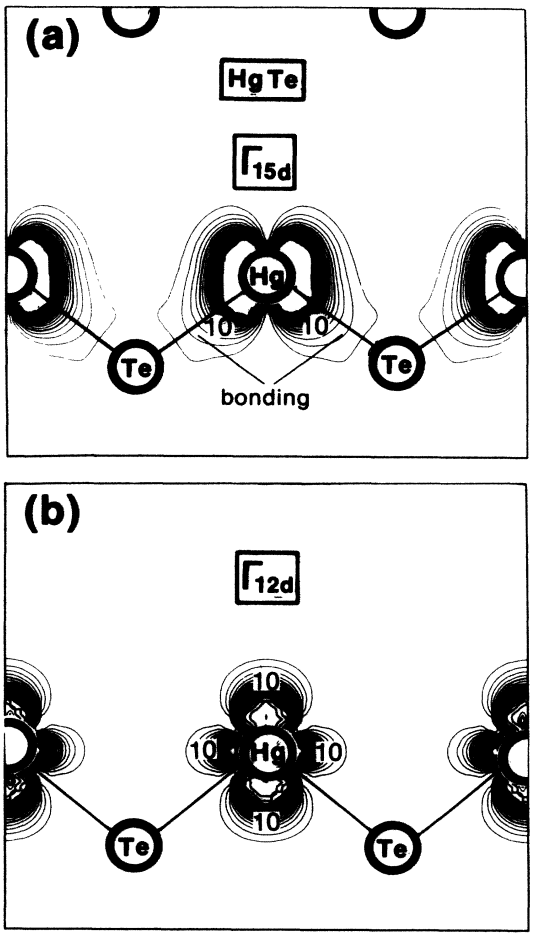

FIG. 10. Wave-function amplitude for *d*-band states in HgTe. (a) Γ_{15d} and (b) Γ_{12d}. Note the bonding buildup of charge along the bond in (a) and the nonbonding character in (b). See caption to Fig. 8 for units.

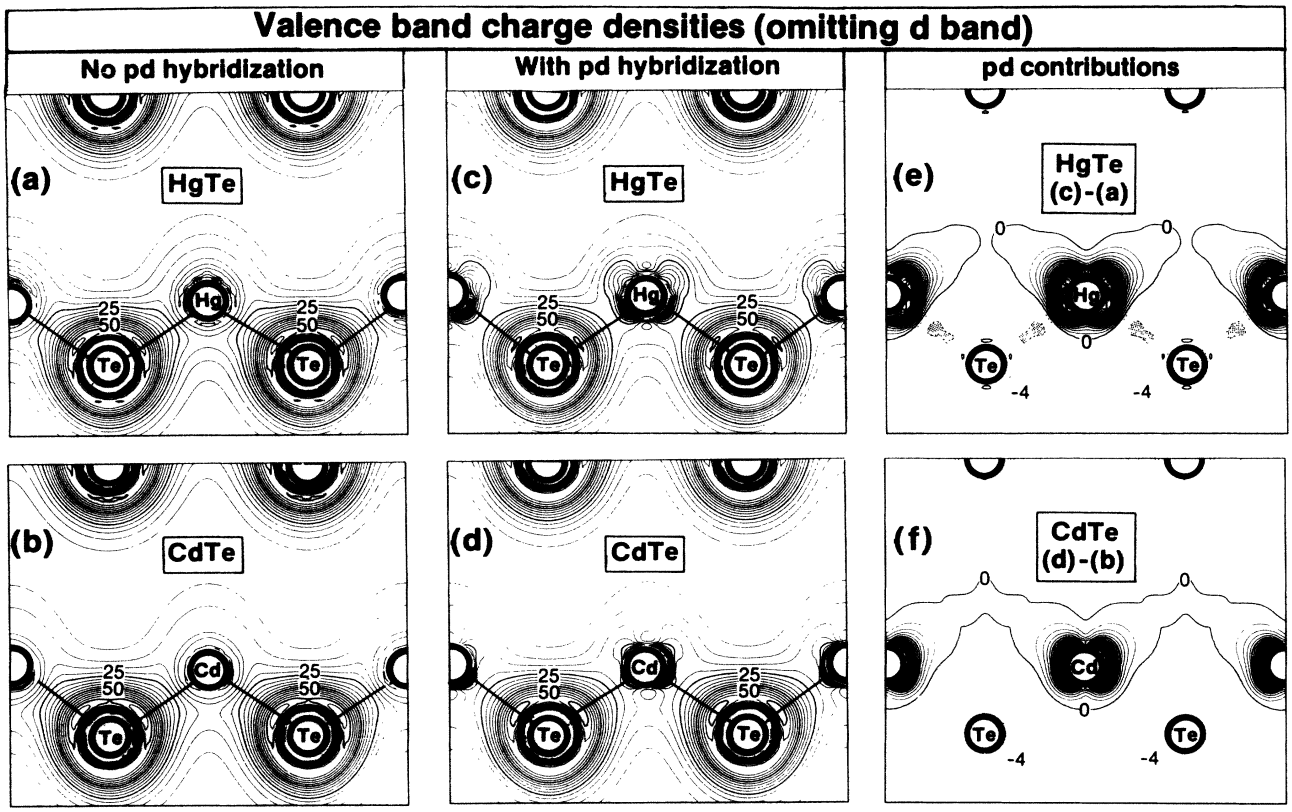

FIG. 11. Comparison of charge density of CdTe and HgTe valence states calculated in (a) and (b) without *p-d* hybridization and in (c) and (d) with *p-d* hybridization (see text). (e) and (f) show the corresponding charge-density differences. For clarity of display the cation *d* bands were omitted. Note in (e) how *p-d* hybridization removes charge from the Hg—Te bond. The charge density is given in units of 10^{-3} *e*/a.u.^{3}. The step sizes are 5 in (a)–(d) and 2 in (e) and (f). The dashed lines indicate negative region. The reduced bond strength in (e) is highlighted by the shaded area.

and HgTe in Figs. 11(c) and 11(d), respectively, while Figs. 11(e) and 11(f) give the differences in charge densities induced by *p-d* repulsion effects. These results show that *p-d* repulsion depletes charge from the cation-anion bond [negative contours, depicted in Figs. 11(e) and 11(f) by dashed lines], and deposits it in the antibonding direction around the cation site [lobes in Figs. 11(e) and 11(f), pointing *towards* the interstitial sites]. It is this *p-d*–repulsion–induced bond weakening (stronger in HgTe, with its shallow and delocalized *d* electrons) which causes the reduction in cohesive energies of these materials (Table X).

C. Spin-orbit splittings

Spin-orbit (SO) splittings exhibit opposite contributions from *p* and *d* orbitals[87,88] and, hence, constitute an interesting measure of the *p-d* hybridization discussed in the preceding section. The spin-orbit Hamiltonian is

$$\hat{H}_{\rm SO}=2\lambda\mathbf{L}\cdot\mathbf{S}=\lambda(J^2-S^2-L^2)\ , \tag{6}$$

where L, S, and J are the angular-, spin-, and total-momentum operators and $\lambda>0$ is the spin-orbit–coupling constant. For fixed S and L, the energy depends only on J, giving the following splittings (Fig. 12):

(i) pure *p* states ($L=1$, $S=\frac{1}{2}$, $J=\frac{3}{2};\frac{1}{2}$),

$$\Delta_p=E[\Gamma_8(J=\tfrac{3}{2})]-E[\Gamma_7(J=\tfrac{1}{2})]=3\lambda_p\ ; \tag{7}$$

(ii) pure *d* states ($L=2$, $S=\frac{1}{2}$, $J=\frac{5}{2},\frac{3}{2}$),

$$\Delta_d=E[\Gamma_8(J=\tfrac{3}{2})]-E[\Gamma_7(J=\tfrac{5}{2})]=-5\lambda_d\ . \tag{8}$$

Hence, in the absence of *p-d* coupling one expects to find the Γ_7 state below the Γ_8 state [Fig. 12(a)] at valence-band maximum, whereas *p-d* coupling [Fig. 12(b)] tends

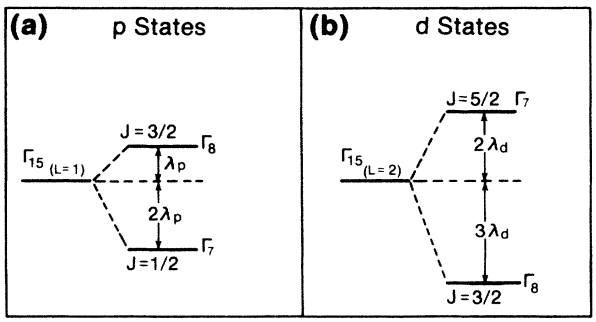

FIG. 12. Schematic plot of the spin-orbit splitting of t_2 states for angular momenta $L=1$ and 2 in tetrahedral symmetry.

to shift Γ_7 upwards.

If p-d mixing is allowed, the splitting can be approximately described[87] as a combination of Δ_p and Δ_d of Eqs. (7) and (8), weighed by the fraction Q_d of the d charge in the state in question (Γ_{15v} here), e.g.,

$$\Delta_0 = E[\Gamma_{8v}] - E[\Gamma_{7v}] \simeq \alpha(1-Q_d)\Delta_p + \beta Q_d \Delta_d \ , \quad (9)$$

where α and β are the geometrical coefficients depending on the charge distribution of the state. In the extreme case of very strong p-d coupling (e.g., in[59] CuCl), one finds a *negative* Δ_0.

We have calculated the spin-orbit splitting Δ_0 (at Γ_{15v}) and Δ_1 (at L_{3v}) directly from the band structure. The results [Δ_0(band calc.) and Δ_1(band calc.)] are given in Table XIII. In addition, we have calculated Δ_0 and Δ_1 from Eq. (9). We find that if we consider Δ_p as the SO splitting of the Γ_{15v} states with no p-d hybridization and Δ_d as the SO splitting of the cation d states, then the coefficients α and β of Eq. (9) approximately satisfy $\alpha(1-Q_d) \simeq \beta \simeq 1$, i.e.,

$$\Delta = \Delta_p + Q_d \Delta_d \ . \quad (10)$$

Results obtained using this equation are also given in Table XIII {denoted Δ[Eq. (10)]}. Our basic conclusions are as follows: (i) Using the fraction of d character (Q_d) obtained from band-structure calculations in Eq. (10) we reproduce nearly the same spin-orbit splitting obtained directly by incorporating H_{SO} of Eq. (6) into the band Hamiltonian. This confirms Eq. (10), demonstrating a *linear reduction* in spin-orbit splitting as the d hybridization increases. (ii) Our LAPW results are in substantial agreement with the LMTO results of Refs. 69 and 70. (iii) Calculated results agree with experiment for ZnTe and CdTe, but disagree with the experimental value[85,89–96] quoted for HgTe (see Table XII). (iv) If p-d coupling is neglected (resulting in the $\Delta_0 = \Delta_p$ values given in the first line of Table XIII), we find better agreement with the current experimental data, or with that calculated by Chadi *et al.*[18(b)] neglecting p-d repulsion [Δ_0(CdTe) = 0.91 eV, Δ_0(HgTe) = 0.94 eV].

TABLE XIII. Calculated spin-orbit splittings at Γ (denoted Δ_0) and L (denoted Δ_1), in eV. Q_d denotes the fraction of d character in the respective wave functions. Δ(band calc.) is the value obtained from direct band-structure results, using the method of Refs. 66. Δ[Eq. (10)] corresponds to the simple approximation of Eq. (10), where the SO splitting is expressed as a difference between the p-orbital contributions Δ_p and the d-orbital contribution $Q_d\Delta_d$. Here, Δ_p is obtained from band calculations when p-d repulsion is removed, and Δ_d is obtained as the splitting of the cation d state when p-d repulsion is included. Δ_d is very close to the value obtained from atomic calculation, which gives −0.35, −0.70, and −1.78 eV for Zn, Cd, and Hg, respectively. For experimental results and data obtained from LMTO calculations, see Table XII.

	ZnTe	CdTe	HgTe
$\Delta_p(\Gamma_{15v})$	0.92	0.90	0.99
Δ_d	−0.37	−0.69	−1.68
$Q_d(\Gamma_{15v})$	0.072	0.074	0.129
Δ_0[Eq. (10)]	0.89	0.85	0.78
Δ_0(band calc.)	0.89	0.86	0.78
$\Delta_p(L_{3v})$	0.54	0.56	0.69
$Q_d(L_{3v})$	0.045	0.045	0.085
Δ_1[Eq. (10)]	0.52	0.53	0.55
Δ_1(band calc.)	0.51	0.53	0.53

The disagreement with experiment for HgTe deserves further attention. The experimental measurement of Δ_0 for HgTe is complicated by its inverted band structure [see Fig. 2(c), showing Γ_{1c} *below* Γ_{15v}]. To our knowledge only indirect measurements[89–96] have been used to deduce Δ_0 for HgTe. For instance, Δ_0 has been deduced from the "$\frac{2}{3}$ rule"[87] ($\Delta_1 \simeq \frac{2}{3}\Delta_0$), by measuring the spin-orbit splitting Δ_1 near the L point, rather than Δ_0 itself. This yielded[89] $\Delta_0 \sim 1.0$ eV for HgTe. However, the "$\frac{2}{3}$ rule" is valid only when noncubic mixing of the p states with cation d states is absent. Because of large p-d hydridization in HgTe, this approach can easily give an error of 0.2 eV in Δ_0. Δ_0 has also been estimated[90–94] by using it as a fitting parameter (along with other adjustable parameters) in theoretical band-structure models for interpretation of experimental data. Using this approach values of Δ_0 ranging from 0.75 eV (Ref. 90) to 0.96 eV (Refs. 91–94) have been obtained for $Hg_{0.2}Cd_{0.8}Te$ and $\Delta_0 = 1.0$ eV (Ref. 89) and 1.10 eV (Ref. 94) for HgTe. Unfortunately, the fitting equations are quite insensitive to the value for Δ_0 in a range as large as ± 0.5 eV,[89] so Δ_0 cannot be determined accurately in this way. Using photoluminescence spectroscopy and resonant Raman scattering, Olego *et al.*[95] recently estimated the upper limit for the difference Δ_0(HgTe) − Δ_0(CdTe) to be 0.12 eV. Since their analysis assumes a valence-band offset ΔE_v(CdTe/HgTe) ~ 0.04 eV, which disagrees with more recent data (0.35 eV, see Sec. VI E), these results are also questionable. Vèrié *et al.*,[96] in their study of band-gap spin-orbit-splitting resonance effects in $Hg_{1-x}Cd_xTe$ alloys, suggest that the resonance should occur at ~0.73 if Δ_0 for HgTe is taken as 1.15 eV.[94] If, instead, we use Δ_0(HgTe) ~ 0.90 eV (as we are predicting), we find that the resonance should occur near $x \sim 0.70$, i.e., the change of resonance composition relative to that determined by Vèrié *et al.*, is quite small. Finally, Δ_0 have been measured for $Hg_{1-x}Cd_xTe$ [Ref. 85(a)] and $Hg_{1-x}Mn_xTe$ [Ref. 85(b)] as a function of composition using the electroreflectance technique. They found Δ_0(HgTe) = 1.08 eV. However, they did not measure E_0 and $\Delta_0 + E_0$ simultaneously. They found an unresolved paradox:[85(a)] if one assumes that the composition variation of E_0 is given by the model of Van Vechten and Bergstesser[97] or by the results of other experiments,[98] anomalous behavior results, i.e., Δ_0 around $x = 0.5$ is even smaller than that of CdTe ($\Delta_0 \sim 0.91$ eV). If, on the other hand, one attempts a reasonable fit to their spectra using Δ_0(HgTe) = 1.08 eV, one must assign in their model an unreasonably large covalent radius for the Hg atom.

On the theoretical side two uncertainties exist. First, in calculating Δ_0 perturbatively from the band structure we assumed that the $j = l + \frac{1}{2}$ and $l - \frac{1}{2}$ radial orbitals can be averaged.[65,66] This approximation could intro-

duce an error of $\lesssim 0.2$ eV for the Hg $6p_{1/2}$ state, so the Hg $6p$ spin-orbit splitting could be underestimated by this amount. Since the Γ_{15v} valence-band maximum of HgTe includes only 6% Hg $6p$ character, the value of Δ_0 is underestimated by ≤ 0.02 eV. This correction can be added to our directly calculated value of Table XIII. The second potential source of error in the theory may arise from the fact that the calculated d-band energies (Table XII) are less bound than photoemission studies indicate (Table I), so that p-d hybridization is overestimated. To examine quantitatively the effect of the position of the cation d band on the spin-orbit splitting, we have repeated a series of self-consistent band-structure calculations for ZnTe, CdTe, and HgTe, artificially moving the cation d bands to deeper binding energies. (This was done by increasing the exchange parameter α which multiplies the exchange potential away from its nominal value of $\frac{2}{3}$ towards 1. Owing to the larger spatial localization of cation d orbitals relative to all other valence states, this scaling moves the cation d bands to more negative energies relative to other states.) Figure 13 depicts the calculated Δ_0 values for ZnTe, CdTe, and HgTe as a function of the separation $E_{d_{3/2}}$ of the cation d band from the valence-band maximum. The vertical arrows denote the observed position of the $d_{3/2}$ states in photoemission experiments (Table I). Evaluating Δ_0 and Δ_1 at these points and adding the estimated correction due to averaging the $l+\frac{1}{2}$ and $l-\frac{1}{2}$ radial orbitals for HgTe, we find the predicted Δ_0 and Δ_1 values to be

$$\begin{aligned} &\Delta_0(\mathrm{ZnTe})=0.94 \text{ eV}, \quad \Delta_1(\mathrm{ZnTe})=0.56 \text{ eV}, \\ &\Delta_0(\mathrm{CdTe})=0.91 \text{ eV}, \quad \Delta_1(\mathrm{CdTe})=0.56 \text{ eV}, \\ &\Delta_0(\mathrm{HgTe})=0.90 \text{ eV}, \quad \Delta_1(\mathrm{HgTe})=0.63 \text{ eV}; \end{aligned} \tag{11}$$

hence,

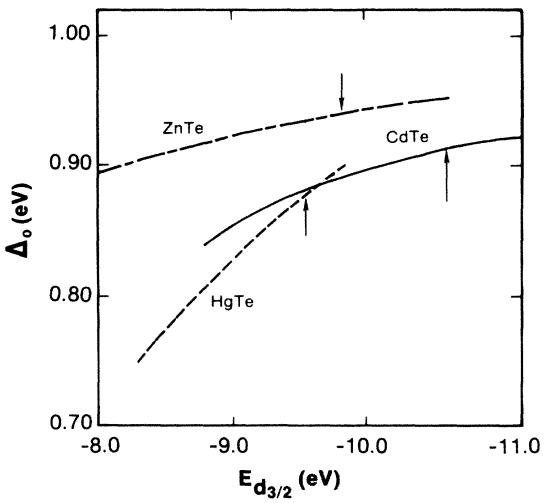

FIG. 13. Variation of spin-orbit splitting Δ_0 as a function of the energy position of the cation $d_{3/2}$ states, $E_{d_{3/2}}$, with respect to the VBM for ZnTe, CdTe, and HgTe. The arrows point to the position of the experimentally observed $E_{d_{3/2}}$ from photoemission (Table I).

$$\Delta_0(\mathrm{CdTe}) \cong \Delta_0(\mathrm{HgTe}), \tag{12}$$

in contrast with the currently accepted experimental results[85] $\Delta_0(\mathrm{HgTe})=1.08$ eV, $\Delta_0(\mathrm{CdTe})=0.90$ eV.

The difference between our predictions of Eq. (12) and the currently accepted experimental values showing $\Delta_0(\mathrm{CdTe}) < \Delta_0(\mathrm{HgTe})$ has an important implication: current interpretations and fittings of Δ_0 have traditionally assumed that Δ_0 of common-anion systems generally increases with the cation atomic number.[88] We find, however, that if p-d mixing exists the opposite can be true, because the conventional analysis disregards p-d-mixing effects which also increase with the cation atomic number and contribute to a *reduction* of Δ_0. *Direct* experimental determinations of Δ_0 for HgTe would be very desirable and would test our predictions [Eqs. (7)–(12)], currently in conflict with the indirectly measured values.

D. Charge distribution in the valence bands and charge redistribution in forming ternary compounds

If the cation d bands in II-VI compounds (dashed areas in Figs. 2 and 3) were dispersionless and chemically inert, omission of their contributions from the total charge density would not alter the charge density in the *bond* region (outside the atomic cores). In this case, one could use the charge densities of the upper valence band alone (topmost ~ 6 eV in Fig. 2) to judge whether, e.g., CdTe has a larger or smaller degree of covalency (charge buildup) on the bond relative to HgTe. To test this hypothesis we show in Figs. 14(a) and 14(b) the calculated charge densities in the upper valence bands of HgTe and CdTe, respectively; Fig. 14(c) gives their difference. We find that this difference has substantial negative values [highlighted by the shaded areas in Fig. 14(c)] on the bond. From this one would judge CdTe to have more electron density on its bond than HgTe, i.e., that CdTe is significantly more covalent than HgTe. This reflects the stronger p-d repulsion in HgTe relative to CdTe, effectively shifting charge in HgTe away from the bond region (compare also Fig. 11). This effect is smaller in CdTe which has a weaker p-d repulsion.

However, the cation d bands in II-VI compounds are extended; the corresponding wave functions [Figs. 14(d) and 14(e)] have an appreciable amplitude in the bond region. Since the Hg $5d$ states are more extended than the Cd $4d$ states [see difference in d-band charge densities in Fig. 14(f)], adding the contribution of these bands to the charge density may alter one's view on the relative covalencies of these two materials. To examine this suggestion, we show in Fig. 15 the *difference* between the charge densities of HgTe and CdTe along the bond direction. As noted from Fig. 14(c), if the contribution of the cation d band to the charge density is omitted, HgTe would be judged to have less density on its bond than CdTe [negative values of $\rho(\mathrm{HgTe})-\rho(\mathrm{CdTe})$ in Fig. 15(a), highlighted as the dashed area]. However, adding the contribution of the cation d bands [Fig. 15(b)] shows that the two materials have *comparable* covalencies (CdTe being slightly more covalent). We conclude that the charge distribution of the cation d states is crucial in determining the co-

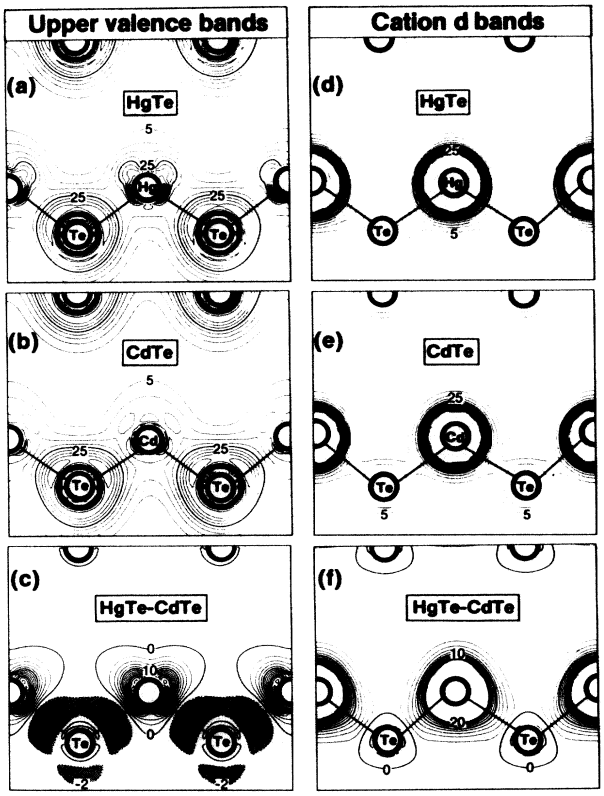

FIG. 14. Charge-density contours for the upper valence bands [(a) and (b)] and the cation *d* bands [(d) and (e)] for CdTe and HgTe. (c) and (f) give their differences. The units are 10^{-3} e/a.u.^{3} The step sizes are 5 for (a), (b), (d), and (e), and 2 for (c) and (f). The shaded regions in (c) indicate negative density differences, highlighting the reduced covalency of HgTe.

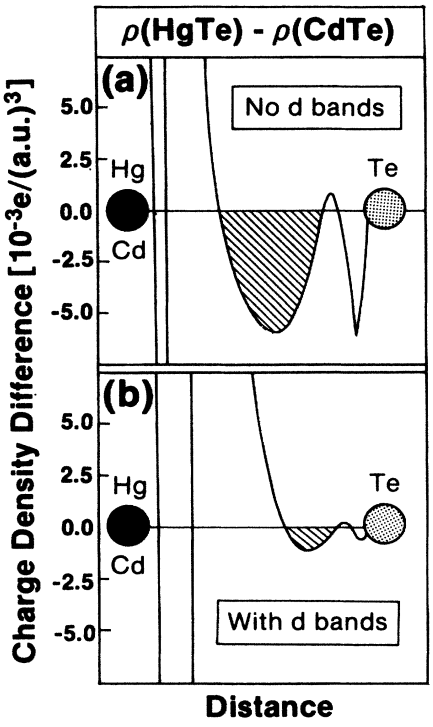

FIG. 15. Valence charge-density difference between HgTe and CdTe along the cation-anion bond direction. (a) Cation *d* bands omitted; (b) cation *d* bands included.

valency of CdTe relative to HgTe.

Current interest in HgTe-CdTe alloys has raised the question of the stability and charge transfer[25,26,78,79] in ordered $Hg_nCd_{4-n}Te_4$ compounds ($n=1,2,3$) relative to the binary constituents ($n=0$ and 4). We have calculated the band structure, total energies, and charge densities of $HgCdTe_2$ ($n=2$ above) in the tetragonal CuAuI-like structure. As discussed in Sec. VI A, we find this ternary compound to have a higher energy per atom than its binary constituents and hence predict that no spontaneous, stable ordering should occur in $Hg_{0.5}Cd_{0.5}Te$ solid solution. To examine the charge redistribution in the ternary compound relative to the binary constituents, we show charge-density differences in Fig. 16 along the bond directions. If the contributions of the cation *d* bands to the charge densities were ignored [Figs. 16(a) and 16(b), denoted "no *d*"], one would have erroneously concluded that in the ternary phase electron charge is *accumulated* on the Hg—Te bond [positive dashed areas in Fig. 16(a)] and *depleted* from the Cd—Te bond [negative dashed areas in Fig. 16(b)]. However, this charge accumulation on the Hg—Te bond in the ternary system is merely an artifact of the omission of the contributions of the cation *d* bands to the charge densities, as evidenced by Figs. 16(c) and 16(d) (which include the effects of the *d* bands), exhibiting *depletion* of charge on the Hg—Te bond [Fig.

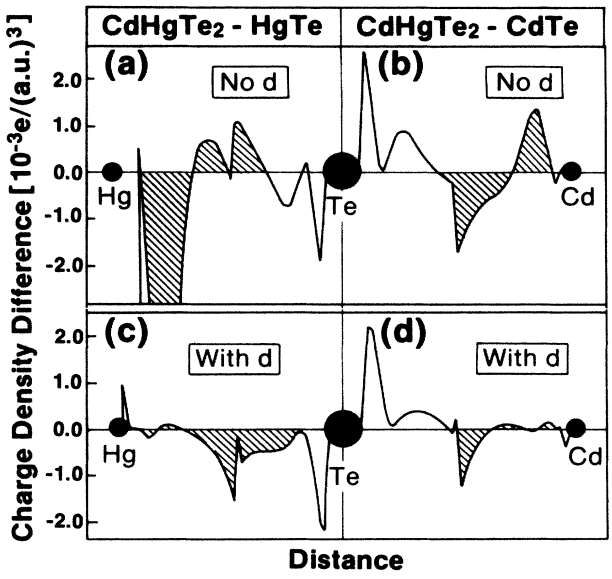

FIG. 16. Valence charge-density difference between $CdHgTe_2$ and its binary constituents CdTe and HgTe along the cation-anion bond directions. (a) and (c) Hg—Te bond; (b) and (d) Cd—Te bond. In (a) and (b) cation *d* bands are removed; in (c) and (d) cation *d* bands are included.

16(c)] and Cd—Te bond [Fig. 16(d)] in forming the ternary phase from its binary constituents. The buildup of charge on the Hg—Te bond in $CdHgTe_2$ in the absence of contributions from the deep d band [Fig. 16(a)] is merely a consequence of a smaller p-d repulsion in $CdHgTe_2$ relative to HgTe. The reduced bond charge on the Hg—Te bond in the real system [Fig. 16(c)] is due to reduced d-orbital bonding in the ternary phase. Using the tight-binding method (which neglects cation d bands) Chen *et al.*[78] have suggested that the reduced Hg—Te bond strength and bond length in the ternary is due to an unfavorable charge transfer from the Cd—Te bond (in a bonding state) to the Hg—Te bond (in an antibonding state), i.e., in a direction opposite to what our calculations show. Their argument is hence not supported by our results, since we find that the charge on the Hg—Te bond is actually *reduced* [Fig. 16(c)]. We also find that the Hg—Te and Cd—Te bond lengths are unchanged (to within 0.001 Å) when the ternary $Hg_nCd_{4-n}Te_4$ phase is formed from its binary constituents.

E. Valence-band offsets between II-VI compounds

The offset $\Delta E_{\rm VBM}$ between the valence-band maxima (VBM) of two semiconductors A and B forming a heterostructure is one of the most important device parameters of interfacial structures.[99] It can be decomposed into an intrinsic "bulk" (b) contribution $\Delta E^b_{\rm VBM}$ characteristic of the two separated systems A and B and an "interface-specific" (IS) contribution $\Delta E^{\rm IS}_{\rm VBM}$ that depends on the properties of the A-B interface:

$$\Delta E_{\rm VBM}=\Delta E^b_{\rm VBM}+\Delta E^{\rm IS}_{\rm VBM} . \tag{13}$$

Tight-binding models[54] have calculated $\Delta E^b_{\rm VBM}$ as the difference between the energies of the Γ_{15v} valence-band maximum [Eq. (3)] of the constituent semiconductors,

$$\Delta E^b_{\rm VBM}(AC/BC)=\varepsilon_{BC}(\Gamma_{15v})-\varepsilon_{AC}(\Gamma_{15v}) . \tag{14}$$

Since common-anion semiconductors have the same anion energy ε^a_p, in this model the difference $\Delta E^b_{\rm VBM}(AC/BC)$ reflects the effect of different cation energies ε^c_p and different matrix elements V_{pp}. Table III reveals, however, that all IIB cations have similar ε^c_p values. Furthermore, the CdTe-HgTe and GaAs-AlAs pairs also have nearly identical bond lengths, hence V_{pp} (which in the tight-bonding model[22(a)] depends solely on bond length) is nearly identical for each member of the pair. Equation (14) would thus predict nearly vanishing $\Delta E^b_{\rm VBM}(AC/BC)$ values for most common-anion semiconductors [$\Delta E^b_{\rm VBM}$(TB) in Table XIV]. This result was codified as the hitherto successful "common-anion rule,"[100] stating that two semiconductors sharing the same anion would have a very small valence-band offset.

The recent experimental discovery that $\Delta E_{\rm VBM}$ is nonzero for ^{101}CdTe-HgTe and ^{102}GaAs-AlAs has focused attention on the second term of Eq. (13). This has recently been modeled in the tight-binding framework[103] as the difference between the average s-p hybrid (h) energies of the two semiconductors, i.e.,

$$\Delta E^{\rm IS}_{\rm VBM}(AC/BC)\simeq\varepsilon_h(AC)-\varepsilon_h(BC) , \tag{15}$$

where $\varepsilon_h(AC)$ is

$$\varepsilon_h(AC)=\tfrac{1}{8}(\varepsilon^a_s+3\varepsilon^a_p+\varepsilon^c_s+3\varepsilon^c_p) . \tag{16}$$

This correction, however, did not change the situation much, as can be seen from Table XIV, which gives the tight-binding results for $\Delta E^b_{\rm VBM}$, $\Delta E^{\rm IS}_{\rm VBM}$, and $\Delta E_{\rm VBM}$ for a few common-anion semiconductors.

The thought underlying the common-anion rule and its representation by tight-binding models was that the valence-band maxima of covalent semiconductors sharing the same structure, lattice constant, and a common anion would exhibit very similar valence-band energies ε_v, or a vanishing valence-band discontinuity ΔE_v. The fallacy in this approach is that valence-band states of common-anion semiconductors manifest *cation* components in addition to anion states. Although such *extravalence* states (e.g., the Al 3d) or *subvalence* states (e.g., Zn, Cd, and Hg

TABLE XIV. Calculated and observed valence-band offsets (in eV), for II-VI semiconductor pairs. The right-hand compound in each pair has the higher VBM. Comparison is given with tight-binding (TB) and Tersoff's results.

	CdTe/ZnTe	CdTe/HgTe	ZnTe/HgTe	MnTe/CdTe
$\Delta E_{\rm VBM}$(with d)[a]	0.13±0.02	0.37±0.03	0.26±0.04	0.25±0.10[b]
Expt.	0.10±0.06[c]	0.35±0.06[d]	0.25±0.05[c]	<0.1[e]
		0.36±0.05[c]		
$\Delta E^b_{\rm VBM}$(TB, no d)[f]	−0.07	0.00	0.07	0.04
$\Delta E^{\rm IS}_{\rm VBM}$(TB, no d)[f]	0.00	0.09	0.09	0.05
$\Delta E_{\rm VBM}$(TB, no d)[f]	−0.07	0.09	0.16	0.09
Tersoff[g]	0.01	0.51	0.50	0.75[h]

[a]Present study, spin-orbit splitting effects are included; see Ref. 56.
[b]Averaged over spin-up and spin-down states.
[c]Reference 104.
[d]Reference 101.
[e]Reference 106.
[f]Reference 105.
[g]Reference 106.
[h]The Mn 3d states are "frozen" in this calculation of Ref. 106.

outer *d* orbitals) were previously thought irrelevant, we have demonstrated through all-electron, first-principles calculations that *these cation d orbitals provide the most important discriminating factor* between a pair of binary common-anion semiconductors and hence control their band offset. We first demonstrate this principle using a simple tight-binding model and then quantitatively calculate the energies involved.

Consider first two binary common-anion semiconductors AX and BX and neglect the effect of d states on the band discontinuity between them [Fig. 17(a)]. The cation p orbitals (A,p) and (B,p) can couple with the anion p orbital (X,p) since all have the same symmetry (t_2, or Γ_{15}) in the zinc-blende lattice. This coupling results in the two bonding states $\Gamma_{15v}(A\text{-}X)$ and $\Gamma_{15v}(B\text{-}X)$, whose energy difference provides—in this model—$\Delta E_v(AX/BX)$. We see that each of these bonding states is repelled to *deeper* energies relative to (X,p) since the cation-p-orbital energy is generally *above* the anion-p-orbital energy. This repulsion

$$V^2(A,p;X,p)/[\varepsilon(A,p)-\varepsilon(X,p)]$$

is proportional to the coupling matrix element $V(A,p;X,p)$ and hence increases as the A—X bond length becomes shorter. If AX and BX have the same bond length and similar cation p energies (as is the case in CdTe-HgTe or AlAs-GaAs), this model predicts a vanishing band offset, in contrast with experiment. This model correctly predicts, however, that the VBM energy of the material with the shorter bond length is smaller than that for the material with the longer bond length, e.g., $\varepsilon_v(\mathrm{Ga}X) < \varepsilon_v(\mathrm{In}X)$.

In many binary materials AX and BX the cation d states cannot be neglected. If these orbitals are *below* the anion p state (e.g., Cu 3*d*, Zn 3*d*, Ag 4*d*, Cd 4*d*, Au 5*d*, or Hg 5*d*), they will repeal *upwards* the valence-band maximum, as shown in Fig. 17(b). Since this repulsion is proportional to

$$V^2(A,d;X,p)/[\varepsilon(X,p)-\varepsilon(A,d)]\ ,$$

it becomes larger as the A—X bond becomes shorter and as the d-orbital energy of the cation A becomes shallower. Hence, since the Hg 5*d* state is shallower than the Cd 4*d* state, HgTe would have a *higher* VBM energy than CdTe. This model leads to finite band offsets between common-anion pairs with the same bond length and similar cation-p-orbital energies, in agreement with experiment. (Note that Al has empty, high-energy 3*d* orbitals which *lower* the VBM in AlAs relative to GaAs.)

We have calculated the valence-band offsets of the four II-VI common-anion semiconductors CdTe/HgTe, CdTe/ZnTe, ZnTe/HgTe, and MnTe/CdTe in a way that parallels their measurement in photoemission core-level spectroscopy.[101] Three quantities are needed in such a calculation (Fig. 18). The core-level binding energies $E^{AC}_{nl,A}=\varepsilon^{AC}_{\mathrm{VBM}}-\varepsilon^{AC}_{nl,A}$ and $E^{BC}_{n'l',B}=\varepsilon^{BC}_{\mathrm{VBM}}-\varepsilon^{BC}_{n'l',B}$ of the cations A and B, respectively relative to the VBM (obtained from the band structures of AC and BC, respectively), and the core-level difference $\Delta E^{A,B}_{nl,n'l'}=\varepsilon_{nl,A}-\varepsilon_{n'l',B}$ [calculated from the band structure of the (001)

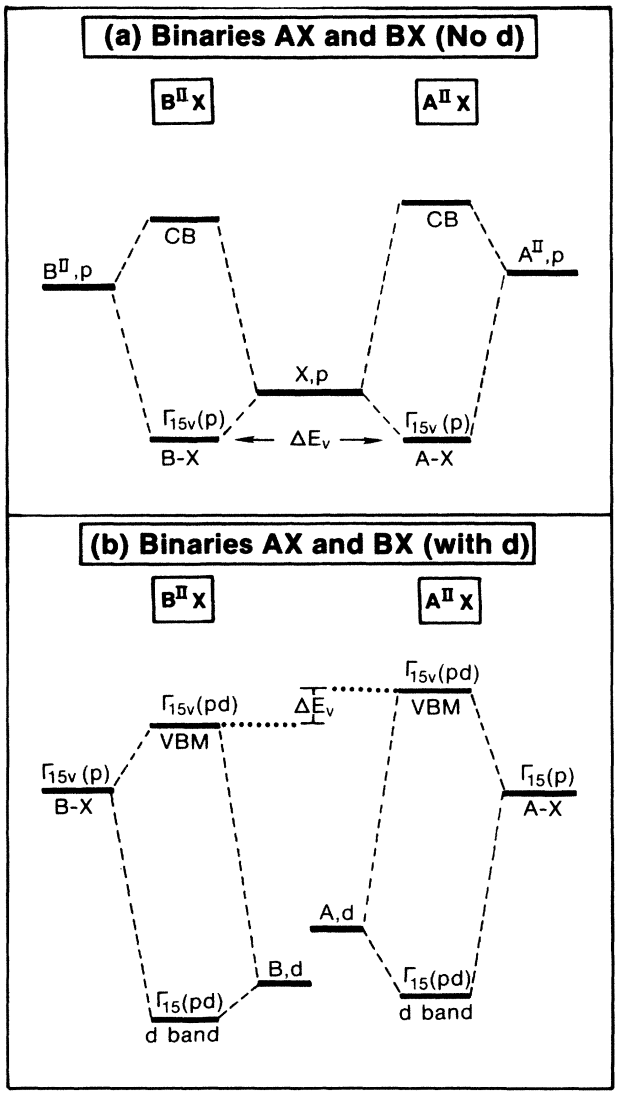

FIG. 17. Energy-level diagram applied to binary semiconductor heterojunctions, (a) neglecting and (b) considering the role of the cation d states. CB indicates conduction band.

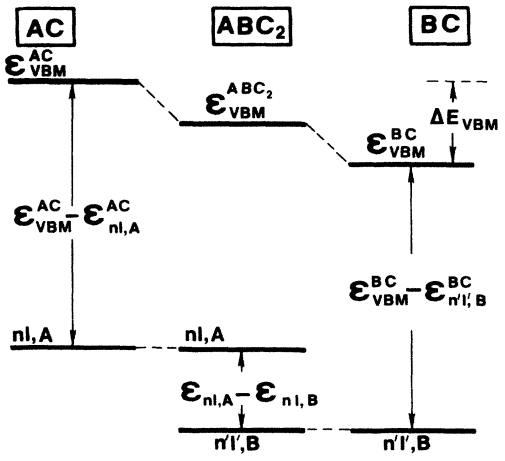

FIG. 18. Schematic energy-level diagram used to deduce the valence-band offset between AC and BC in our calculation.

$(AC)_1(BC)_1$ superlattice, which is equivalent to the ABC_2 "CuAuI" structure]. We have shown,[56] using a simple electrostatic model, that for common-anion systems interface dipole effects are small and localized near the interface, so that an ultrathin superlattice is appropriate to obtain the core-level difference $\Delta E^{A,B}_{nl,n'l'}$. The valence-band offset $\Delta E_{\rm VBM}$ is then obtained as

$$\Delta E_{\rm VBM} \cong E^{AC}_{nl,A} - E^{BC}_{n'l',B} + \Delta E^{A,B}_{nl,n'l'} \ . \tag{17}$$

Including p-d hybridization we find calculated valence-band offsets in good agreement with experimental data.[101,104] Our results (with d) are compared with tight-binding (TB) calculation[105] (no p-d repulsion) and experimental data[101,104,106] for CdTe/ZnTe, CdTe/HgTe, ZnTe/HgTe, and MnTe/CdTe in Table XIV. We also listed results obtained by Tersoff,[107] whose theory emphasizes the importance of the interface dipole contribution to the valence-band offset. Our results and analysis suggest that the interface dipole effects are small for these systems.

VII. SUMMARY

We have demonstrated that the existence of a fully occupied, nominally "nonbonding" d band inside the valence band of II-VI semiconductors affects the properties of these systems near the valence-band maximum. The incomplete screening by the d electrons of the core leads to profoundly different properties of IIB-VI compounds relative to IIA-VI compounds, lacking this d shell. In addition, the d electrons have a *direct* effect on the other orbitals of the system, due to the symmetry-allowed p-d interaction. These effects involve the following:

(i) Reduction of the direct band gap due to upward repulsion of the Γ_{15v} state by the d bands at lower energies.

(ii) Reduction of the spin-orbit splitting.

(iii) Reversal of the order of the d-orbital Γ_{15} and Γ_{12} states relative to the prediction of point-ion crystal-field models.

(iv) Deepening of the Cu acceptor states in II-VI compounds, leading to high-resistivity response.

(v) Reduction of the band gap and spin-orbit splitting of ternary chalcopyrites relative to the analogous II-VI compounds.

(vi) Inverted exchange splitting in ferromagnetic zinc-blende MnTe.

(vii) Reduction in the cohesive energy and increase in the lattice parameters of II-VI compounds.

(viii) Introduction of antibonding character in the charge distribution of the upper valence bands.

(ix) Reduction of the difference in covalent character between HgTe and CdTe.

(x) Significant increase in the valence-band offset between common-anion II-VI pairs (e.g., CdTe-HgTe).

We further predict that p-d repulsion will lead to a near equality of the spin-orbit splitting at Γ_{15v} of CdTe and HgTe, in contrast with the currently accepted result $\Delta_0(\text{HgTe}) > \Delta_0(\text{CdTe})$.

ACKNOWLEDGMENT

This work was supported by Office of Energy Research, Materials Science Division, U.S. Department of Energy, under Grant No. DE-AC02-77-CH00178.

APPENDIX: TIGHT-BINDING MODELS FOR ESTIMATING ΔE_{pd}

Accurate isolation of the p-d repulsion energy $\Delta E_{pd} = \Gamma_{15v}(pd) - \Gamma_{15}(p)$ in a solid is difficult because the atomic p and d orbitals are normalized (e.g., compressed) in the solid-state environment and cannot be uniquely separated. However, basic trends can be observed by calculating ΔE_{pd} semiquantitatively using simple tight-binding models. Two of the approaches used in our study will be described.

1. The two-level p-d repulsion model

If one neglects cation p states, the problem of Fig. 4(b) simplifies to a two-level system with anion energy ε_p and cation energy ε_d. In this approach the bonding (b) and antibonding (ab) states have the energies

$$\varepsilon^{\rm b,ab}_{pd} = \frac{\varepsilon_p + \varepsilon_d}{2} \pm \left[\left[\frac{\varepsilon_p - \varepsilon_d}{2} \right]^2 + V^2_{pd} \right]^{1/2} \ . \tag{A1}$$

The fractional d charge in the antibonding $\Gamma_{15}(pd)$ state is

$$Q_d = 1 - \left[1 + \left[\frac{\varepsilon^{\rm ab}_{pd} - \varepsilon_p}{V_{pd}} \right]^2 \right]^{-1} , \tag{A2}$$

and the p-d repulsion energy ΔE_{pd} is given by

$$\Delta E_{pd} = \varepsilon^{\rm ab}_{pd} - \varepsilon_p \ . \tag{A3}$$

In Eqs. (A1)–(A3), ε_p and ε_d are the orbital energies of the unperturbed p and d states, respectively, and V_{pd} is the coupling matrix element. The problem with this approach is that V_{pd} is difficult to calculate reliably. Furthermore, it is doubtful that neutral-atom orbital energies can be used for the d states since the intra-atomic Coulomb repulsion energy is large for such states. To get around these difficulties we note that Eqs. (A1)–(A3) can be rearranged to yield

$$\begin{aligned} \varepsilon^{\rm ab}_{pd} - \varepsilon^{\rm b}_{pd} &= E[\Gamma_{15v}(pd) - \Gamma_{15d}(dp)] \\ &= 2 \left[\frac{(\varepsilon_p - \varepsilon_d)^2}{4} + V^2_{pd} \right]^{1/2} \end{aligned} \tag{A4}$$

$$Q_d = 1 - \left[1 + \left[\frac{\Delta E_{pd}}{V_{pd}} \right]^2 \right]^{-1} , \tag{A5}$$

$$E[\Gamma_{15v}(pd) - \Gamma_{15d}(dp)] = (\varepsilon_p - \varepsilon_d) + 2\Delta E_{pd} \ , \tag{A6}$$

i.e., where $(\varepsilon_p - \varepsilon_d)$, ΔE_{pd}, and V_{pd} are unknowns, but Q_d and $E[\Gamma_{15v}(pd) - \Gamma_{15d}(dp)]$ are easily accessible: the energy difference $E[\Gamma_{15v}(pd) - \Gamma_{15d}(dp)]$ can be obtained

directly from our band-structure calculation and, similarly, the fractional d character Q_d in the $\Gamma_{15v}(pd)$ state can also be estimated from the band wave functions (Table XI). Solving Eqs. (A4)–(A6) simultaneously, we obtain V_{pd} and ΔE_{pd}. The results are listed in Table V. The major error in this approach is the uncertainty in Q_d (since it depends on the choice of the muffin-tin size and on the way in which the d basis functions are constructed). Three choices have been tried in our calculation: (1) define Q_d as the charge inside the cation MT sphere with angular momentum $l=2$ character for the Γ_{15v} state, (2) take Q_d to be the averaged value of the cation d charge in the Γ_{15v} state and the anion p charge in the Γ_{15d} state, and (3) as in (1) above, but calculate Q_d with the $d_{3/2}$-state binding energy adjusted to be the experimental value (see Sec. VI C). We see from Table V that in all three cases V_{pd} is of the order of 2 eV, and that although these three models give a scatter (of ~ 0.3 eV) in the absolute values of ΔE_{pd}, the *relative* change $\delta_{pd}=\Delta E_{pd}^{AC}-\Delta E_{pd}^{BC}$ has only a small scatter (see Table VI).

2. ΔE_{pd} calculated from total valence-band width

In this approach ΔE_{pd} is estimated by comparing the calculated total valence-band width when d states are included ($W_{\rm tot}^{\rm calc}$, obtained from the present LAPW calculation) and the width obtained in the absence of d bands ($W_{\rm tot}^{\rm TB}$, TB calculation with sp states only), i.e.,

$$\Delta E_{pd}=W_{\rm tot}^{\rm calc}-W_{\rm tot}^{\rm TB} \tag{A7}$$

and

$$W_{\rm tot}^{\rm calc}=\Gamma_{15v}(pd)-\Gamma_{1v}(s)\ , \tag{A8}$$

$$W_{\rm tot}^{\rm TB}=\left[\frac{\varepsilon_p^c+\varepsilon_p^a}{2}-\left[\frac{(\varepsilon_p^c-\varepsilon_p^a)^2}{4}+V_{pp}^2\right]^{1/2}\right] -\left[\frac{\varepsilon_s^c+\varepsilon_s^a}{2}-\left[\frac{(\varepsilon_s^c-\varepsilon_s^a)^2}{4}+V_{ss}^2\right]^{1/2}\right], \tag{A9}$$

where ε_p^c, for example, is the atomic-orbital energy of the cation p states and V_{pp} and V_{ss} are the coupling constants.

Harrison[49(c)] has argued that for s and p states in semiconductors the interatomic and intra-atomic Coulomb interactions nearly cancel each other; hence neutral-atom orbital energies can be used. The uncertainty in this calculation is that his universal coupling parameters[22(a),49(b)] are fitted to a particular set of atomic eigenvalues. In our calculation we tried both Harrison's "old"[22(a)] and "new"[49(b)] parameters (models B1 and B2 in Table VII). We used our calculated semirelativistic LDF atomic eigenvalues in order to be consistent with the band-structure calculations. The results are given in Table VII. Again we see that the relative change δ_{pd} (Table VIII) is rather insensitive to the parameters used in the calculations.

From these two model calculations we find that ΔE_{pd} can be substantial ($\sim 0.5-1$ eV) in II-VI compounds and that whereas the difference of p-d repulsion energy δ_{pd} for the CdX/ZnX pair is small, it is large for the pairs involving Hg, i.e., CdX/HgX and ZnX/HgX.

[1] N. J. Shevchik, J. Tejeda, M. Cardona, and D. W. Langer, Phys. Status Solidi B **59**, 87 (1973).

[2] L. Ley, R. A. Pollak, F. F. Mcfeely, S. P. Kowalczyk, and D. A. Shirley, Phys. Rev. B **9**, 600 (1974).

[3] (a) C. J. Veseley, R. L. Hengehold, and D. W. Langer, Phys. Rev. B **5**, 2296 (1972); (b) E. P. Domashevskaya and V. A. Terekhov, Phys. Status Solidi B **105**, 121 (1981); (c) V. Formichev, T. M. Zimkina, and I. I. Zhukovn, Fiz. Tverd. Tela (Leningrad) **10**, 3073 (1968) [Sov. Phys.—Solid State **10**, 2421 (1969)].

[4] D. J. Stukel, R. N. Euwema, T. C. Collins, F. Herman, and R. L. Kortum, Phys. Rev. **179**, 740 (1969).

[5] F. Herman, R. L. Kortum, C. D. Kuglin, and J. L. Shay, in *II-VI Semiconducting Compounds*, edited by D. G. Thomas (Benjamin, New York, 1967), p. 503; F. Herman, R. L. Kortum, C. D. Kuglin, J. P. Van Dyke, and S. Skillman, in *Methods of Computational Physics* (Academic, New York, 1968), p. 193.

[6] P. Eckelt, O. Madelung, and J. Treusch, Phys. Rev. Lett. **18**, 656 (1967); J. Treusch, P. Eckelt, and O. Madelung, in *II-VI Semiconducting Compounds*, Ref. 5, p. 558; H. Overhof, Phys. Status Solidi B **45**, 315 (1971).

[7] A. Zunger and A. J. Freeman, Phys. Rev. B **17**, 4850 (1978).

[8] C. S. Wang and B. M. Klein, Phys. Rev. B **27**, 3393 (1981).

[9] P. Bendt and A. Zunger, Phys. Rev. B **26**, 3114 (1982).

[10] J. E. Bernard and A. Zunger, Phys. Rev. B **36**, 3199 (1987); **34**, 5992 (1986).

[11] S.-H. Wei and A. Zunger, Phys. Rev. B **35**, 2340 (1987).

[12] M. L. Cohen and T. K. Bergstresser, Phys. Rev. **141**, 789 (1966).

[13] M. L. Cohen, in *II-VI Semiconducting Compounds*, Ref. 5, p. 462.

[14] F. Aymerich, F. Meloni, and G. Mulor, Phys. Rev. B **15**, 3980 (1977); F. Aymerich, A. Baldereschi, and F. Meloni, in Proceedings of the 4th International Conference on Ternary and Multinary Compounds, Tokyo, 1980 [Jpn. J. Appl. Phys. **19**, (Suppl. 19-3), 161 (1980)].

[15] (a) J. R. Chelikowsky and M. L. Cohen, Phys. Rev. B **14**, 556 (1976); (b) R. M. Wentzcovitch, S. L. Richardson, and M. L. Cohen, Phys. Lett. **114A**, 203 (1986); (c) J. R. Chelikowsky, Solid State Commun. **22**, 351 (1977).

[16] J. R. Chelikowsky, D. J. Chadi, and M. L. Cohen, Phys. Rev. B **8**, 2786 (1973).

[17] (a) J. D. Joannopoulos and M. L. Cohen, J. Phys. C **6**, 1572 (1973); (b) M. L. Cohen, Science **179**, 1189 (1973); (c) J. P. Walter and M. L. Cohen, Phys. Rev. B **4**, 1877 (1971).

[18] (a) J. P. Walter, M. L. Cohen, Y. Petroff, and M. Balkanski, Phys. Rev. B **1**, 2662 (1970); (b) D. J. Chadi, J. P. Walter, M. L. Cohen, Y. Petroff, and M. Balkanski, *ibid.* **5**, 3058 (1972).

[19] J. Ihm and M. L. Cohen, Phys. Rev. B **20**, 729 (1979); W. E. Pickett and M. L. Cohen, *ibid.* **18**, 939 (1978); W. E. Pickett, S. G. Louie, and M. L. Cohen, Phys. Rev. Lett. **39**, 109 (1977); J. R. Chelikowsky and M. L. Cohen, Phys. Rev. B **13**, 826 (1976).

[20]K. C. Hass and D. Vanderbilt, in *Proceedings of the 18th International Conference on the Physics of Semiconductors,* edited by O. Engström (World Scientific, Singapore, 1987); p. 1181; J. Vac. Sci. Technol. A **5**, 3019 (1987).

[21]K. J. Chang, S. Froyen, and M. L. Cohen, Phys. Rev. B **28**, 4736 (1983).

[22](a) W. A. Harrison, *Electronic Structure and the Properties of Solids* (Freeman, San Francisco, 1980); (b) J. Vac. Sci. Technol. B **3**, 1231 (1985).

[23]D. J. Chadi and M. L. Cohen, Phys. Status Solidi B **68**, 49 (1975).

[24]P. Vogl, H. P. Hjalmarson, and J. D. Dow, J. Phys. Chem. Solids **44**, 365 (1983).

[25]A. B. Chen and A. Sher, Phys. Rev. B **32**, 3695 (1985).

[26]A. Sher, A. B. Chen, W. E. Spicer, and C. K. Shih, J. Vac. Sci. Technol. A **3**, 105 (1985).

[27]K. C. Hass, H. Ehrenreich, and B. Velicky, Phys. Rev. B **27**, 1088 (1983).

[28]D. J. Chadi, Phys. Rev. B **16**, 790 (1977).

[29]M. Podgorny and M. T. Czyzyk, Solid State Commun. **32**, 413 (1974).

[30]A. B. Chen and A. Sher, Phys. Rev. B **31**, 6490 (1985).

[31]P. Pecheur, J. van der Rest, and G. Toussaint, J. Cryst. Growth **72**, 147 (1985); P. H. Meijer, P. Pecheur, and G. Toussaint, Phys. Status Solidi B **140**, 155 (1987).

[32]P. Vogl, in *Festkörperproblem XXI (Advances in Solid State Physics),* edited by P. Grosse (Pergamon/Vieweg, Braunchsweig, 1981), p. 191.

[33]R. W. G. Wykoff, *Crystal Structures,* 2nd ed. (Interscience, New York, 1963), Vol. 1, pp. 86–90.

[34]P. W. Bridgman, Proc. Am. Acad. Arts Sci. **74**, 21 (1940). These are the averaged bulk moduli between 0 and 0.5 GPa. For BaS, see S. Yamaoka, O. Shimomura, H. Nakazawa, and O. Fukunaga, Solid State Commun. **33**, 87 (1980).

[35]O. Kubachevski and C. B. Alcock, *Metallurgical Thermochemistry,* 5th ed. (Pergamon, New York, 1979), pp. 267–322.

[36]C. Kittel, *Solid State Physics,* 5th ed. (Wiley, New York, 1975), p. 74.

[37]W. H. Strehlow and E. L. Cook, J. Phys. Chem. Ref. Data **2**, 163 (1973). Results for ZnO are given by D. G. Thomas, J. Phys. Chem. Solids **15**, 86 (1960).

[38]N. Kh. Abrikosov, V. B. Bankina, L. V. Poretskaya, L. E. Shelimova, and E. V. Skudnova, *Semiconducting II-VI, IV-VI, and V-VI Compounds* (Plenum, New York, 1969), p. 2.

[39]*Landolt-Börnstein: Numerical Data and Functional Relationships* in Science and Technology, edited by O. Madelung (Springer-Verlag, Berlin, 1982), Vol. 17b.

[40]A. F. Wells, *Structural Inorganic Chemistry,* 4th ed. (Clarendon, Oxford, 1975), p. 911.

[41]A. R. West, *Solid State Chemistry and Its Applications* (Wiley, Chichester, 1986), p. 230.

[42]B. N. Figgis, *Introduction to Ligand Fields* (Interscience, New York, 1966), pp. 74–106.

[43]J. E. Huheey, *Inorganic Chemistry,* 3rd ed. (Harper and Row, New York, 1983).

[44]C. E. Moore, *Ionization Potentials and Ionization Limits Derived from the Analysis of Optical Spectra,* NSRDS–Nat. Bur. Stand. (U.S.) Circ. No. 34 (U.S. GPO, Washington, D.C., 1971).

[45]If the II*B*-VI compounds had the rocksalt structure, their cubic lattice constants would have been even smaller than those reported in Table II, since the rocksalt structure is more compact.

[46]J. C. Phillips, Phys. Rev. Lett. **27**, 1197 (1971).

[47]H. Watanabe, *Operator Methods in Ligand Field Theory* (Prentice-Hall, Englewood Cliffs, NJ, 1966), p. 87.

[48]A. Zunger, in *Solid State Physics,* edited by H. Ehrenreich and D. Turnbull (Academic, New York, 1980), Vol. 39, p. 275.

[49](a) C. F. Fischer, Atomic Data **4**, 301 (1972). For the extrapolated *p* orbital energies of II*B* atoms, see (b) W. A. Harrison, Phys. Rev. B **24**, 5835 (1981); (c) **31**, 2121 (1985).

[50]F. Herman and S. Skillman, *Atomic Structure Calculations* (Prentice-Hall, Englewood Cliffs, NJ, 1963). Also see Ref. 22(a) for the extrapolated *p*-orbital energies of II*B* atoms.

[51]L. Hedin and B. I. Lundqvist, J. Phys. C **4**, 2063 (1971).

[52]N. J. Shevchik, J. Tejeda, and M. Cardona, Phys. Rev. B **9**, 2627 (1974).

[53]r_d for Zn, Cd, and Hg are extrapolated from Harrison's Solid State Table in Ref. 22(a). They are 0.63, 0.86, and 0.98 Å, respectively.

[54]W. A. Harrison, J. Vac. Sci. Technol. **14**, 1016 (1977).

[55]J. A. Van Vechten, Phys. Rev. **187**, 1007 (1964). See, however, improved results in J. A. Van Vechten, J. Vac. Sci. Technol. B **3**, 1240 (1985).

[56]S.-H. Wei and A. Zunger, Phys. Rev. Lett. **59**, 144 (1987); J. Vac. Sci. Technol. B **5**, 1239 (1987).

[57]L. F. Mattheiss, Phys. Rev. B **5**, 290 (1972); **5**, 306 (1972). In these papers, however, Mattheiss had argued that the Γ_{12} state could be lower in energy than the $P_{25'}$ state in rocksalt structure since e and t_2 band energies are not related in a simple way to Γ_{12} and $\Gamma_{25'}$ states. We find this to be the case for CdTe and HgTe in their high-pressure rocksalt phases.

[58](a) A. Zunger and M. L. Cohen, Phys. Rev. B **20**, 1189 (1979); (b) A. Blacha, N. E. Christensen, and M. Cardona, *ibid.* **33**, 2413 (1986).

[59]A. Goldmann, Phys. Status Solidi B **81**, 9 (1977). For an early determination of the invertal spin-orbit splitting in CuCl, see M. Cardona, Phys. Rev. **129**, 69 (1963).

[60]Y. S. Park and B. K. Shin, in *Electroluminescence,* edited by J. Pankov (Springer, Berlin, 1977), p. 133.

[61]J. E. Jaffe and A. Zunger, Phys. Rev. B **29**, 1882 (1984).

[62]J. L. Shay and J. H. Wernick, *Ternary Chalcopyrites Semiconductors: Growth, Electronic Properties and Applications* (Pergamon, Oxford, 1975), pp. 118–120.

[63]S.-H. Wei and H. Krakauer, Phys. Rev. Lett. **55**, 1200 (1985), and references therein.

[64]P. Hohenberg and W. Kohn, Phys. Rev. **136**, B864 (1964); W. Kohn and L. J. Sham, *ibid.* **140**, A1133 (1965).

[65]D. D. Koelling and B. N. Harmon, J. Phys. C **10**, 3107 (1977).

[66]A. H. MacDonald, W. E. Pickett, and D. D. Koelling, J. Phys. C **13**, 2675 (1980); W. E. Pickett, A. J. Freeman, and D. D. Koelling, Phys. Rev. B **23**, 1266 (1981).

[67]D. J. Chadi and M. L. Cohen, Phys. Rev. B **8**, 5747 (1973).

[68]S.-H. Wei, A. A. Mbaye, L. G. Ferreira, and A. Zunger, Phys. Rev. B **36**, 4163 (1987).

[69]N. E. Christensen and O. B. Christensen, Phys. Rev. B **33**, 4739 (1986).

[70]N. A. Cade and P. M. Lee, Solid State Commun. **56**, 637 (1985).

[71]R. Juza, A. Rabenau, and G. Pascher, Z. Anorg. Allg. Chem. **285**, 61 (1956).

[72]B. Segall, M. R. Lorentz, and R. E. Halsted, Phys. Rev. **129**, 2471 (1963).

[73]J. C. Wooley and B. Ray, J. Phys. Chem. Solids **13**, 151 (1960).

[74]D. Berlincourt, H. Jaffe, and L. R. Shiozawa, Phys. Rev. **129**, 1009 (1963).

[75]R. Dornhaus and G. Nimitz, in *Narrow-Gap Semiconductors,* edited by G. Höhler and E. A. Niekisch (Springer-Verlag,

New York, 1983), p. 126.
[76]A. Fazzio, M. J. Caldas, and A. Zunger, Phys. Rev. B **30**, 3430 (1984).
[77]W. A. Harrison, J. Vac. Sci. Technol. A **1**, 1672 (1983).
[78]A.-B. Chen, A. Sher, and W. E. Spicer, J. Vac. Sci. Technol. A **3**, 1674 (1985). These authors have calculated the cohesive energies of CdTe and HgTe, both assuming neutral-atom orbital energies (obtaining E_c values of 4.44 and 2.08 eV/pair for CdTe and HgTe, respectively) and by assuming that the on-site orbital energies vary linearly with atomic charge (obtaining considerably smaller E_c values of 2.95 and 0.61 eV/pair for CdTe and HgTe, respectively). The experimental results (Table IX) are $E_c(\mathrm{CdTe})=4.45$ ev and $E_c(\mathrm{HgTe})=3.22$ eV. However, in the second calculation the authors have failed to include the Madelung correction that acts to offset the on-site variation of orbital energies with charge. This correction will act to considerably alter the results, as noted in Ref. 49(c).
[79]A. Sher, M. A. Merding, S. Krishnamurthy, M. van Schilfgaarde, A.-B. Chen, and W. Chen, Mater. Res. Symp. Proc. (to be published).
[80]A. V. Savitskii, M. V. Kurik, and K. D. Tovstyuk, Opt. Spektrosk. **19**, 115 (1965) [Opt. Spectrosc. (USSR) **19**, 59 (1965)].
[81]D. G. Thomas, J. Appl. Phys. **32**, 2298 (1961).
[82]Y. Guldner, C. Rigaux, M. Grynberg, and A. Mycielski, Phys. Rev. B **8**, 3875 (1973).
[83]M. Cardona and D. L. Greenaway, Phys. Rev. **131**, 98 (1963).
[84]D. T. Marple and H. Ehrenreich, Phys. Rev. Lett. **8**, 87 (1962).
[85](a) A. Moritani, K. Taniguchi, C. Hamaguchi, and J. Nakai, J. Phys. Soc. Jpn. **34**, 79 (1973); (b) P. M. Amirtharaj, F. H. Pollak, and J. K. Furdyna, Solid State Commun. **39**, 35 (1981).
[86]M. Cardona and G. Harbeke, Phys. Rev. Lett. **8**, 90 (1962).
[87]M. Cardona, in *Modulation Spectroscopy,* Suppl. 11 of Solid State Physics, edited by F. Seitz, D. Turnbull, and H. Ehrenreich (Academic, New York, 1969), pp. 65–73. See also K. S. Song, J. Phys. (Paris) Colloq. Suppl. **28**, C3/C4-195 (1967).
[88]J. C. Phillips, in *Bonds and Bands in Semiconductors* (Academic, New York, 1973), pp. 178–187.
[89]S. H. Groves, R. N. Brown, and C. R. Pidgeon, Phys. Rev. **161**, 779 (1967).
[90]G. A. Antcliffe, Phys. Rev. B **2**, 345 (1970).
[91]H. Kahlert and G. Bauer, Phys. Rev. Lett. **30**, 1211 (1973).
[92]B. D. McCombe, R. J. Wagner, and G. A. Prinz, Phys. Rev. Lett. **25**, 87 (1970).
[93]M. A. Kinch and D. D. Buss, J. Phys. Chem. Solids **32**, 461 (1971).
[94]C. Verie and E. Decamps, Phys. Status Solidi **9**, 797 (1965).
[95]D. J. Olego, J. P. Faurie, and P. M. Raccah, Phys. Rev. Lett. **55**, 328 (1985).
[96]C. Verie, F. Raymond, J. Besson, and T. N. Duy, J. Cryst. Growth **59**, 342 (1982).
[97]J. A. Van Vechten and T. K. Bergstresser, Phys. Rev. B **1**, 3351 (1970).
[98]J. L. Schmit and E. L. Stelzer, J. Appl. Phys. **40**, 4865 (1969).
[99]For a review, see R. Bauer and G. Margaritondo, Phys. Today **40**(1), 26 (1987); M. Kroemer, in *Proceedings of the NATO Advanced Study Institute on Molecular Beam Epitaxy and Heterostructures, Erice, Sicily, 1983,* edited by L. L. Chang and K. Plogg (Nijhoff, The Hague, The Netherlands, 1984).
[100]J. O. McCaldin, T. C. McGill, and C. A. Mead, Phys. Rev. Lett. **36**, 56 (1976).
[101]S. P. Kowalczyk, J. T. Cheung, E. A. Kraut, and R. W. Grant, Phys. Rev. Lett. **56**, 1605 (1986).
[102]W. I. Wang and F. Stern, J. Vac. Sci. Technol. B **3**, 1280 (1985).
[103]W. A. Harrison and J. Tersoff, J. Vac. Sci. Technol. B **4**, 1068 (1986).
[104]T. M. Duc, C. Hsu, and J. P. Faurie, Phys. Rev. Lett. **58**, 1127 (1987).
[105]The tight-binding results are obtained using our semirelativistic local-density orbital eneries (Ref. 56) and the coupling constant of Ref. 49(b).
[106]M. Pessa and O. Jylhä, Appl. Phys. Lett. **45**, 646 (1984).
[107]J. Tersoff, Phys. Rev. Lett. **56**, 2755 (1986).

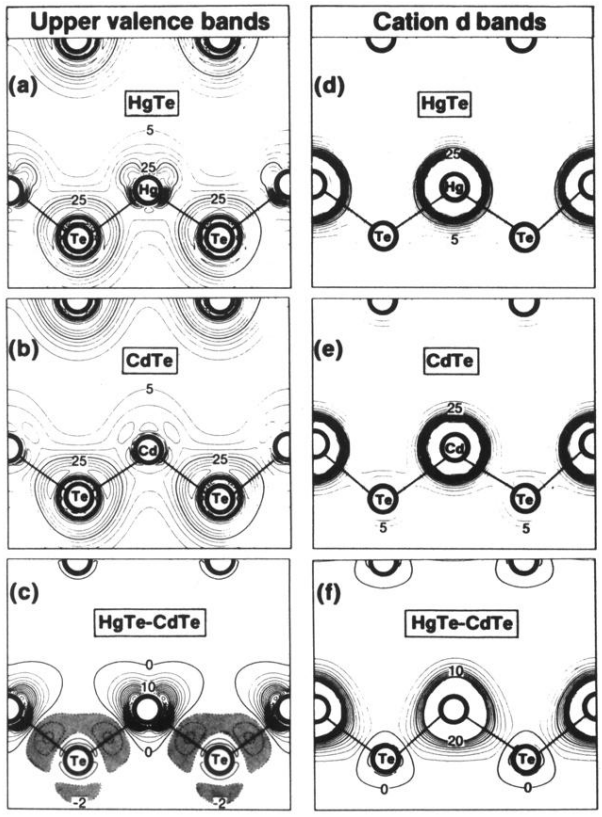

FIG. 14. Charge-density contours for the upper valence bands [(a) and (b)] and the cation d bands [(d) and (e)] for CdTe and HgTe. (c) and (f) give their differences. The units are 10^{-3} e/a.u.^{3} The step sizes are 5 for (a), (b), (d), and (e), and 2 for (c) and (f). The shaded regions in (c) indicate negative density differences, highlighting the reduced covalency of HgTe.

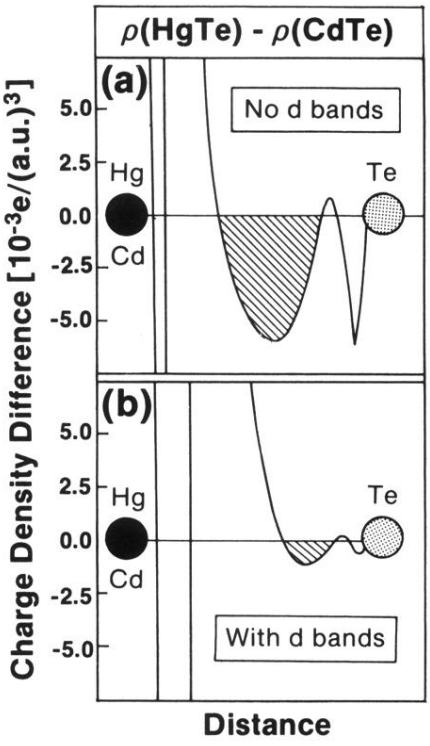

FIG. 15. Valence charge-density difference between HgTe and CdTe along the cation-anion bond direction. (a) Cation *d* bands omitted; (b) cation *d* bands included.

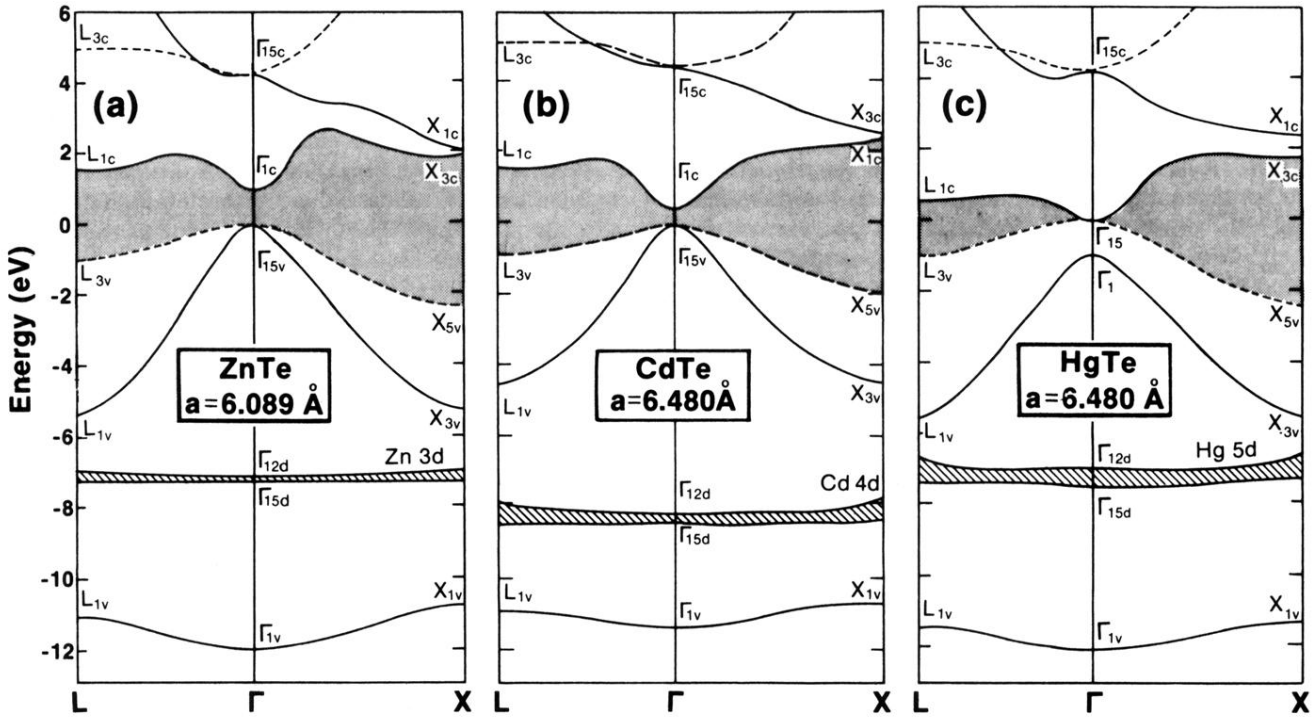

FIG. 2. Calculated (LAPW) band structure of (a) ZnTe, (b) CdTe, and (c) HgTe near their equilibrium lattice constants. The cation *d* bands are highlighted by the dashed lines. The band-gap regions are shaded. Dashed lines indicate doubly degenerate states.

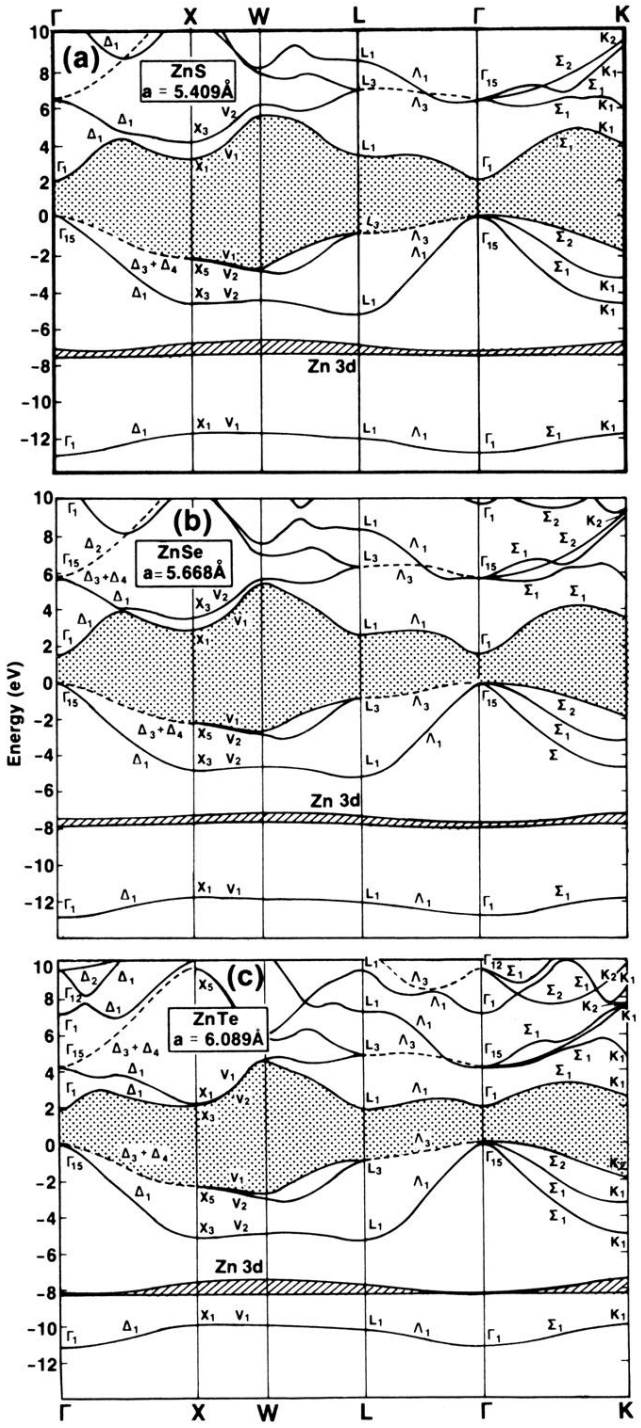

FIG. 3. Same as Fig. 2, but calculated using the nonrelativistic all-electron mixed-basis method (Ref. 10) for (a) ZnS, (b) ZnSe, and (c) ZnTe.

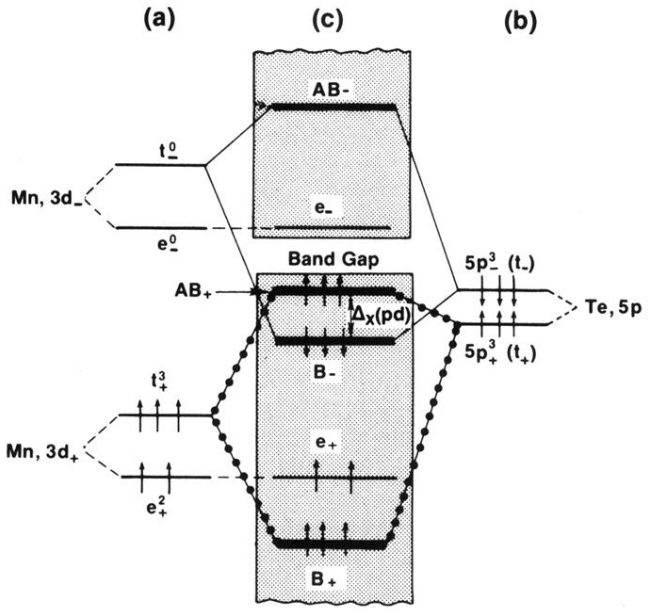

FIG. 7. Schematic diagram of the *p-d*–repulsion effects for the hypothetical ferromagnetic zinc-blende MnTe. (a) Exchange and crystal-field splitting of Mn 3*d* states, (b) exchange splitting of Te 5*p* states, and (c) the final interacting states. Shaded areas denote the host crystal bands. B_+ and B_- denote bonding states for spin up and spin down, respectively, whereas AB_+ and AB_- denote antibonding states for spin up and spin down, respectively. Note how *p-d* repulsion leads here to a negative *p-d* exchange splitting $\Delta_x(pd)$ (i.e., B_- is below AB_+).